KfK 5008
März 1992

Numerical Study of a 50 kA Superconducting Bus for the NET/ITER Model Coil Test in TOSKA-Upgrade

R. Heller
Institut für Technische Physik
Projekt Kernfusion

Kernforschungszentrum Karlsruhe

KERNFORSCHUNGSZENTRUM KARLSRUHE

Institut für Technische Physik

Projekt Kernfusion

KfK 5008

Numerical study of a 50 kA superconducting bus for the NET/ITER model coil test in TOSKA-Upgrade

R. Heller

Kernforschungszentrum Karlsruhe GmbH, Karlsruhe

Kernforschungszentrum Karlsruhe GmbH
Postfach 3640, 7500 Karlsruhe 1

ISSN 0303-4003

Abstract

Based on the design of the superconducting bus bar system for the 1.8 K test of the EURATOM LCT coil in the TOSKA Upgrade facility, a superconducting bus bar was designed for the NET/ITER model coil test for an operating current of 50 kA made out of a NbTi cable-in-conduit-conductor imbedded in a copper profile for electrical and mechanical stabilization. For safety reasons, the mass flow through the bus bar is designed as a separate circuit, i.e. the mass flow rates of the coil pancakes, the bus bar, and the current lead are independently adjustable.

This results in a bus bar which is safe in case of loss of cooling. But the eddy current losses generated in the stabilizing copper during the fast discharge of the model coils are by far too high, i.e. the bus bar will quench during high magnetic field changes.

Therefore, alternatives are discussed in which the design principles of the bus bar were not changed but it was tried to reduce the eddy current losses in the copper stabilizer in two different ways. First, a smaller stabilizing copper profile ($\alpha = 15$ instead of 80) was used, and second, the eddy current losses were reduced by using a so-called PSI-type stabilizer, i.e. a stabilizer made of copper-nickel coated copper wires which are twisted and pressed together to get a rigid profile. But the reduction of the eddy current losses by using these types of copper profile was not high enough, i.e. the bus bars quench during high magnetic field changes.

Therefore, the only possible alternative is a superconducting bus bar consisting of a cable-in-conduit(-CIC)-conductor without any stabilizing copper profile around it. The CIC is imbedded in a jacket made of stainless steel for mechanical stability. The calculations show that this type of bus bar has a high safety margin with respect to AC-losses. The maximum temperature is below the critical temperature of the NbTi superconductor in case of a fast energy dump. The disadvantage is that the cable-in-conduit bus bar has only a small safety margin in case of loss of mass flow if no energy dump of the model coils is initiated immediately.

In any case, the final design has to be a compromise between the safety margin in case of loss of mass flow and the safety margin in case of fast magnetic field changes. This has been used for a proposal for a superconducting bus bar, which has reasonable AC losses, acceptable transient temperature slopes in case of loss of mass flow, and no high temperatures during quench.

The crucial point of the design will be a quench detection system which has to be able to detect few mV.

In this report, the different designs will be described, and the computational results will be presented.

Numerische Studie einer supraleitenden Stromschiene für den NET/ITER Modellspulentest in TOSKA Upgrade

Zusammenfassung

Ausgehend vom Design der supraleitenden Stromschiene für den 1.8 K Test der EURATOM LCT-Spule in der TOSKA Upgrade-Anlage wurde für den NET/ITER Modellspulentest eine Stromschiene für einen Betriebsstrom von 50 kA ausgelegt, die aus einem NbTi "cable-in-conduit" Leiter besteht, welcher zur elektrischen und mechanischen Stabilisierung von einem Kupferprofil umgeben ist. Der Heliumkühlkreis der Stromschiene ist von denen der Spule und der Stromzuführung getrennt, wodurch die Sicherheit erhöht wird.

Berechnungen, die mit den Programmen CURLEAD und HOTSPOT gemacht wurden, zeigen, daß die supraleitende Stromschiene zwar im Fall eines Kühlmittelverlustes eine große Sicherheitsmarge besitzt, das große Volumen an Stabilisierungskupfer jedoch dazu führt, daß in der Stromschiene im Fall einer Schnellentladung bzw. einer Plasmaabrißsimulation eine Temperatur von mehr als 20 K erreicht wird, was zu einem Quench führt.

Als Konsequenz wurde versucht, zum einen das Kupfervolumen zu reduzieren (von einem Kupfer-Supraleiterverhältnis von 80 auf eines von 15), zum anderen eine Segmentierung einzuführen auf eine Weise, wie sie von PSI für deren NET-TF-Leiterentwurf vorgeschlagen worden ist. Beide Modifikationen führen zu keiner drastischen Verbesserung der Stabilität.

Zuletzt wurde das Stabilisierungskupfer ganz durch eine Stahlhülle ersetzt, welche die mechanischen Kräfte aufnehmen kann, durch die jedoch kein elektrischer Strom fließt. Im Fall eines Quenches wirkt der Stahl als zusätzliche Wärmekapazität. Diese Sammelschiene ist stabil genug gegen schnelle Magnetfeldänderungen, besitzt allerdings nur eine kleine Sicherheitsmarge im Fall eines Kühlmittelverlustes.

Wie die endgültige Auslegung aussehen wird, hängt davon ab, welche Priorität die (gegenläufigen) Anforderungen, die an das supraleitende Stromschienensystem gestellt werden, haben.

Es wird ein Vorschlag gemacht, wie die supraleitende Stromschiene aussehen könnte. Er führt zu einem Design, der akzeptable Wechselfeldverluste im Fall einer Spulenentladung bringt, der Temperaturanstieg im Leiter ist tolerabel und die maximale Temperatur, welche während eines Quenches erreicht wird, ist akzeptabel (etwa 70 K).

Der kritische Punkt der Auslegung ist das Quench-Detektions-System, welches einige wenige mV erkennen muß.

In diesem Bericht werden die verschiedenen Auslegungen diskutiert und die Rechenergebnisse vorgestellt und miteinander verglichen.

Table of Contents

List of Illustrations

List of Tables

1. Introduction

The TOSKA Upgrade facility is foreseen for testing model coils wound from conductors proposed for the superconducting toroidal and poloidal field coils of the **N**ext **E**uropean **T**orus, **NET**, resp. the **I**nternational **T**hermonuclear **E**xperimental **R**eactor, **ITER**. The model coils are assembled as a solenoidal stack in TOSKA. The concept definition and present analysis of the NET model coils is described in [1]. Figure 1 shows an artist view of the model coil stack including two double pancakes. The figure was created by using the input data for the computer code EFFI [2].

For the different scenarios proposed for the test, five current leads are needed which should carry a nominal current of 50 kA to reach a maximum field at the conductor of the inner coils of the coil stack of about 13.5 T, whereas the outer coils have a maximum field of 12.5 T.

50 kA is the maximum current the power supply can achieve. To reach the operational, i.e. mechanical and/or electrical limits a scenario is planned which allows a temporary increase of the current in one coil by decreasing the current in the others. The maximum current one can get is 70 kA within 30 seconds.

During normal operation only four current leads are needed whereas the fifth one works in stand-by operation (defined as zero current operation).

To simulate different so-called "normal operation conditions", special current scenarios are forseen, i.e.

- nominal field operation,
- plasma disruption simulation,
- plasma initiation simulation,
- plasma ramp up and slow control simulation, and
- AC loss divertor sweeping and nuclear heating simulation.

The different scenarios are quoted in [1] where also the computed losses are given for one type of conductor proposed for NET/ITER.

Of course, the current lead should be able to discharge the coil in case of the loss of mass flow in the lead without generating too much heat at the connection to the superconducting bus, i.e. at least the coil should not quench. The design of the current leads are described in [3].

In this report, different designs of a superconducting bus bar will be presented which connects the different model coils and the current leads. Because the cooling circuit of the superconducting bus and the current lead will be separated, it was not possible to compute the behaviour of the whole lead and bus system. The solution of the problem will be described in the next section.

All the requirements set to the leads must be fulfilled also by the superconducting bus bar system. Special attention should be given to the loss of helium mass flow because the bus bar system will be cooled with an additional coil flow path, i.e. not by the current lead flow path [4]. With other words, a loss of coolant of the coil itself will result in a loss of coolant of the bus bar system. This has to be designed such that the coil can be discharged in a safe manner.

An additional requirement is the limit on the contact resistance between the coil terminal and the bus bar resp. the bus bar and the current lead which both have to be not more than 10^{-9} Ω. The reason is the limited refrigerator power and the large number of connections, i.e. 21. The technical realisation will not be discussed in this report.

Attention has been paid to the question how stable the superconducting bus bar system is against large field gradients, i.e. how large are the losses generated by the eddy currents originated by the magnetic field changes, e.g. during energy dump or during pulsed operation.

In this report, five different types of bus bar designs will be given, and the computational results concerning the steady-state and transient behaviour, e.g. loss of mass flow will be presented. The

importance having contact resistances of about 1 nΩ are discussed by means of the first type of bus bar presented.

The five types can be characterized as follows:

- A superconducting bus bar scaled from the 1.8 K test of the EURATOM LCT coil having a high total copper to non-copper ratio of about 80. This bus bar is called **SCBUS**.
- A superconducting bus bar having the same copper to non-copper ratio like the SCBUS but made out of copper wires with a copper-nickel coating forming a rigid profile. This bus bar is called **CONIBUS**.
- A superconducting bus bar like the SCBUS with a smaller copper stabilizer cross-section having a total copper to non-copper ratio of 15. This bus bar is called **LCOBUS**.
- A superconducting bus bar like the SCBUS but with no copper stabilizing profile around the cable having a copper to non-copper ratio of 2.5. This type of bus bar is called **CICBUS**.
- The computational results of the latter four types of bus bars lead to the proposal for the superconducting bus bar for the model coil test in TOSKA Upgrade. It consists of a large number of strands with a copper to non-copper ratio of 1.35 imbedded in a jacket made of stainless steel. This bus bar is called **NETBUS**.

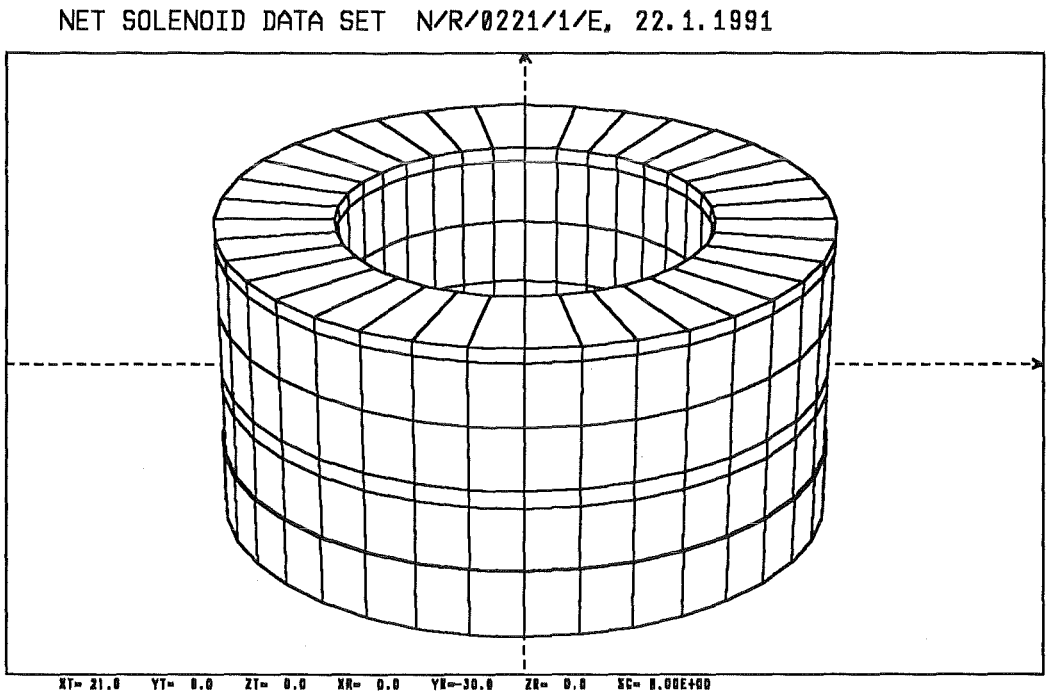

Figure 1. Artist view of the model coil stack including two double pancakes

2. Boundary conditions for the design of a superconducting bus bar

Table 1 shows the input requirements for the design of the superconducting bus bar. Due to the geometrical configuration, the range of the background magnetic field generated by the model coils will be in the order of 2.5 - 4.0 T at the location area of the bus bar. This has been verified by computing the magnetic field at the location area of the superconducting bus bars. Figure 2 shows a contour plot of the magnetic field of the model coils where the location area of the superconducting bus bars is indicated as a box. In Figure 3 the magnitude of the magnetic field is plotted at the location of the bus bar resp. the current lead. In addition the nominal field as used in the calculations has been shown.

Parameter	Unit	Value
Background magnetic field	T	2.5 - 4.0
Nominal current	kA	50
Current region	kA	0 - 70
Average length	m	3.0
Inlet temperature of conductor $T_{Cu,bottom}$	K	5.5
Inlet temperature of helium $T_{He,bottom}$	K	4.5
Top temperature of conductor $T_{Cu,top}$	K	variable
Outlet temperature of helium $T_{He,top}$	K	variable
Inlet pressure of helium	bar	5 - 10
Maximum temperature of conductor after quench $T_{Cu,max}$	K	150
RRR of conductor		50

Table 1. Input parameters for the superconducting bus

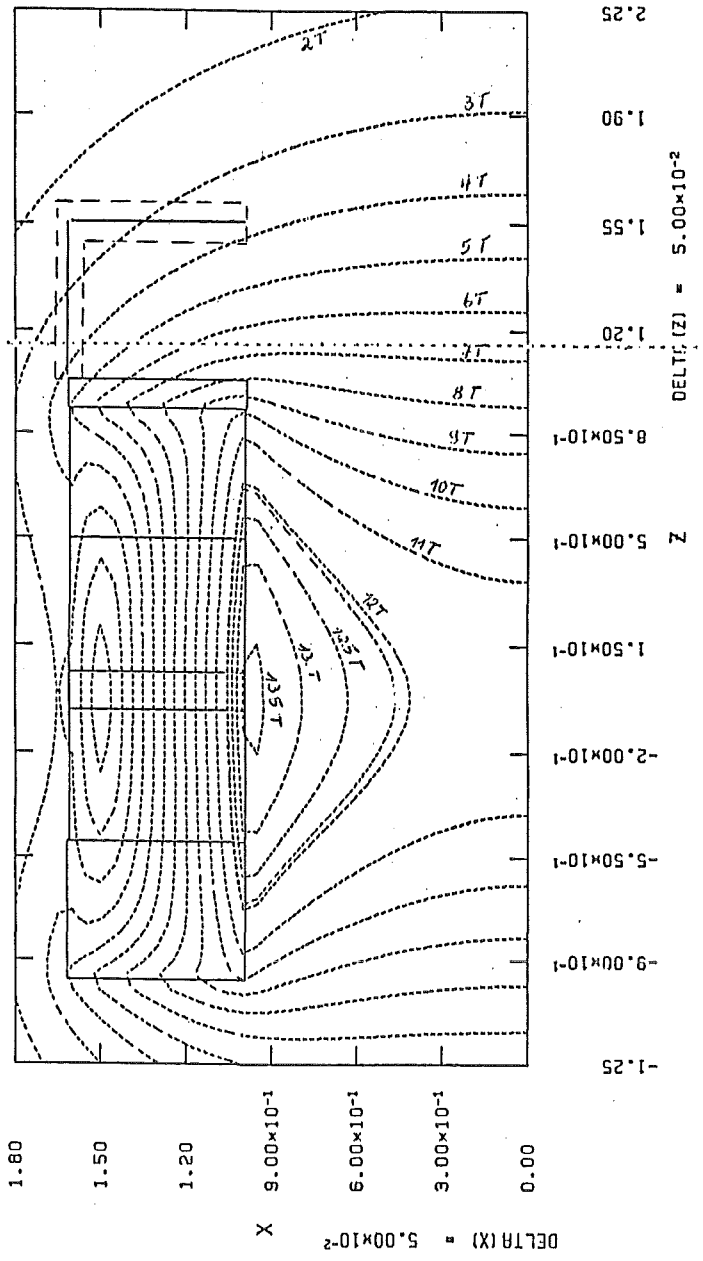

Figure 2. Contour plot of the magnetic field of the model coil stack: The location area of the superconducting bus bars is indicated in the figure as an L-shape on top of the coils

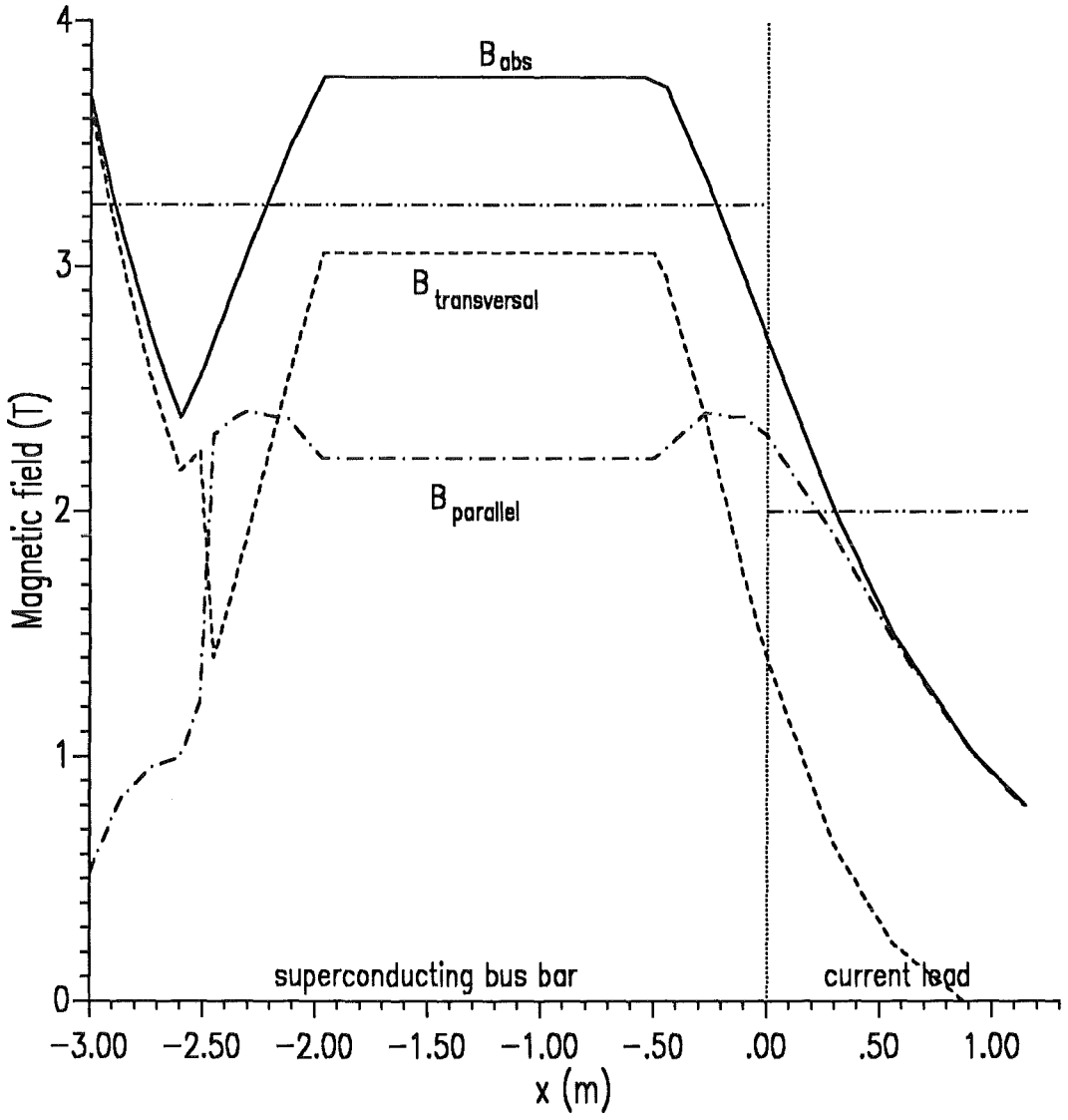

Figure 3. Magnetic field at the location of the superconducting bus bar resp. the current lead: The full line denotes the absolute value of the magnetic field. The transversal (dashed line) resp. parallel (dash-dotted line) field component has been plotted, too. For comparison the average field value as used in the calculations has been added

An important requirement for the superconducting bus bar is the safety margin with respect to AC losses. Three different types of losses have to be investigated, i.e.

- hysteresis losses in the superconductor,
- coupling losses in the copper matrix resp. between the twisted wires in the different cable stages, and
- eddy current losses in the stabilizers, i.e. copper or stainless steel.

In literature, different formulas exist for the calculation of the AC losses. Here, a set of equations is used which represents the losses in terms of energy per conductor volume. For more details see e.g. [5] [6].

a) Hysteresis losses due to transversal field change:

$$Q_{H,t} = \frac{2}{3\pi} j_c(6.2T,3.8K)\, d\, \lambda \int \dot{B}_t dt$$

where
j_c = critical current,
d = filament diameter,
$\lambda = A_{sc}/A_{wire}$,
A_{sc} = superconductor cross section,
A_{wire} = wire cross section.

b) Hysteresis losses due to parallel field change:

$$Q_{H,p} = \frac{1}{6\pi} j_c(6.2T,3.8K)\, d\, \lambda \int \dot{B}_p dt$$

The expressions for the hysteresis losses are only valid for magnetic field changes much larger than the penetration field of the filaments.

c) Coupling losses due to transversal field change:

The coupling losses in the superconductor depend on the way to build up the cable, i.e. the number of cable stages. The way to calculate is the same for the strand itself (due to the twisting of the filaments) as well as for the (sub-)cables (due to the twisting of the wires).

$$Q_{C,t} = \frac{n_s \tau}{\mu_0} \int \dot{B}_t^2 dt$$

where

$$\tau = \frac{1}{2} \mu_0 \frac{l_p^2}{4\pi^2} \frac{1}{\rho_t}$$

where
n_s = cable stage
τ = time constant of the loop,
l_p = twist pitch,
ρ_t = transversal resistivity of the loop, and
$\mu_0 = 4\pi \cdot 10^{-7}$ Vs/Am.

The transversal resistivity of a wire (strand) can be expressed in the following way if the contact resistance between matrix and filament is small compared to that of the matrix. This is true for rather large filaments ($> 30\ \mu$) [7].

$$\rho_t = \frac{1-\lambda}{1+\lambda} \rho_{matrix}$$

where
ρ_{matrix} = resistivity of the copper matrix.

For rather small filaments, the contact resistance between matrix and filament is large compared to that of the matrix. Then the following relation can be used ([7]).

$$\rho_t = \frac{1 + \lambda}{1 - \lambda} \rho_{matrix}$$

For the coupling between the wires, the transversal resistivity of the multiwire stage is mainly determined by the contact resistivity between the wires.

Coupling losses due to transversal field change for a sinoidal field:

The coupling losses in the superconductor due to a sinoidal varying magnetic field change are quoted in [6]. Here the following expression is used (in terms of Joule per conductor volume and cycle) for which the time integration of the magnetic field change is been done.

$$Q_{C,t} = \frac{2\pi B_0^2 \omega\tau}{\mu_0 (1 + \omega^2\tau^2)}$$

where
B_0 = amplitude, and
ω = angular frequency of the sinoidal field change.

d) Coupling losses due to parallel field change:

There exists no formula for the coupling loss due to a parallel field change. The experience shows that the parallel component will be in general smaller than the transversal one. For the calculation of the total losses, it will be assumed that the calculation of the parallel coupling losses will be done using the same formula as for the transversal ones.

e) Eddy current losses in the jacket due to transversal field change:

$$Q_{E,t} = \frac{\tau}{\mu_0} \frac{A_{jacket}}{A_{wire}} \int \dot{B}_t^2 dt$$

$$\tau = \frac{1}{12} \mu_0 \frac{a^3 b - c^3 d}{ab - cd} \frac{1}{\rho}$$

where
τ = time constant of the jacket,
A_{jacket} = jacket cross section,
A_{wire} = wire cross section,
a, b = outer length of the jacket,
c, d = inner length of the jacket,
ρ = resistivity of the jacket.

Eddy current losses due to transversal field change for a sinoidal field:

The eddy current losses in the superconductor due to a sinoidal varying magnetic field change can be quoted analogously to the coupling losses. The following expression will be used (in terms of Joule per conductor volume and cycle) for which the time integration of the magnetic field change

$$Q_{E,t} = \frac{2\pi B_0^2 \omega\tau}{\mu_0 (1 + \omega^2\tau^2)} \frac{A_{jacket}}{A_{wire}}$$

where
B_0 = amplitude, and
ω = angular frequency of the sinoidal field change.

f) Eddy current losses in the jacket due to parallel field change:

$$Q_{E,p} = \frac{\tau}{\mu_0} \frac{A_{jacket}}{A_{wire}} \int \dot{B}_p^2 dt$$

$$\tau = \frac{1}{15} \mu_0 \left[\frac{a^3 b^3}{a^2 + b^2} - \frac{c^3 d^3}{c^2 + d^2} \right] \frac{1}{ab - cd} \frac{1}{\rho}$$

For the calculations of the different types of AC losses, the magnetic field changes have to be known at the position of the superconducting bus for each type of scenario sketched in the introduction.

In Figure 3, the transversal and the parallel components of the magnetic field are plotted vs. position at the location of the superconducting bus bar resp. the current lead for the nominal operation, i.e. four model coils and the central double pancake have the nominal current to get a maximum field of 13.5 T at the inner radius of the central double pancake. Due to the change in orientation, the field components show a jump.

From Figure 10, average numbers are obtained for the absolute value of the magnetic field as well as for the components. Table 2 contains the numbers.

	B_{abs} [T]	$B_{transversal}$ [T]	$B_{parallel}$ [T]
Model coil (maximum field)	13.5	13.5	0.0
Superconducting bus bar (average field)	3.25	2.5	2.0
Current lead (average field)	2.0	0.6	1.9

Table 2. Magnetic field values at the model coils, the superconducting bus bar resp. current lead

The magnetic field changes with time can be computed, i.e. $\int \dot{B}\, dt$ resp. $\int \dot{B}^2\, dt$, if the time behaviour of the field is known. This depends on the kind of scenario investigated (see section 1). Because the magnetic field has a linear dependence on the current, it is possible to calculate the integrals shown above analytically. During test operation in TOSKA Upgrade, four kinds of field changes will occur:

- exponential decay due to energy dump
- linear ramp up and down (nuclear heating simulation)
- discharging of one model coil and therefore charging of the others for simulating fast magnetic field changes, i.e. plasma disruption
- sinoidal sweeping due to the ripple of the power supply

a) Exponential decay of the coil current:

Using the exponential behaviour of the current during energy dump leads to the following expressions

$$\int_0^\infty \dot{B} dt = B_0$$

resp.

$$\int_0^\infty \dot{B}^2 dt = B_0^2 \frac{1}{2T_{dump}}$$

where
B_0 = magnetic field at t=0s,
T_{dump} = dump time constant.

b) Linear ramp up and down of the coil current:

Using the linear increase / decrease of the coil current, leads to the following expressions

$$\int_0^{T\bullet} \dot{B} dt = 2 B_0$$

resp.

$$\int_0^{T\bullet} \dot{B}^2 dt = 4 \frac{B_0^2}{T}$$

where
B_0 = magnetic field change amplitude, and
T = cycle time.

c) Sinoidal sweeping of the coil current:

Using the sinoidal behaviour of the current, leads to the following expression

$$\int_{t_a}^{t_e\bullet} \dot{B} dt = 4 B_0$$

where
B_0 = amplitude of the magnetic field change.

In the following, the behaviour of the superconducting bus during an energy dump of the model coils will be investigated.

But first, the effect of the magnetoresistance on the steady-state temperature distribution as well as the effect of different contact resistances on the cooling behaviour of the superconducting bus bar will be presented. The computations are done for the so-called SCBUS.

3. Effect of different contact resistances on the cooling bahaviour

3.1 Boundary conditions due to material properties

The high background magnetic field at the location of the superconducting bus bar resp. the current lead leads to the necessity of using the magnetoresistance of the OFHC copper resp. a lower current sharing resp. critical temperature of the NbTi superconductor. Table 3 summarizes the different current sharing resp. critical temperatures and the critical current densities of NbTi and Nb_3Sn. These numbers have been obtained by using a code containing properties of various materials written by L. Bottura [8].

Parameter	Unit	0.0 T	1.5 T	2.5 T	4.0 T	5.5 T
NbTi (j_{op} = 909 A/mm²)						
T_{cs}	[K]	8.14	7.53	7.10	6.43	5.71
T_c	[K]	9.30	8.74	8.35	7.74	7.10
j_c (B,4.5K)	[A/mm²]	3770	3190	2810	2240	1694
j_c (B,5.0K)	[A/mm²]	3380	2810	2440	1900	0369
j_c (B,5.5K)	[A/mm²]	2980	2440	2080	1550	1043
Nb_3Sn (ε=0.3 %, j_{op} = 2500 A/mm²)						
T_{cs}	[K]	14.91	12.00	10.65	8.70	6.24
T_c	[K]	15.65	14.60	13.91	12.86	13.91
j_c (B,4.5K)	[A/mm²]	37800	9680	7210	5020	3068
j_c (B,5.0K)	[A/mm²]	36200	9230	6850	4730	2920

Table 3. Current sharing temperature, critical temperature, and critical current density of superconductors used

Figure 4 shows the electrical resistivity of copper with an RRR of 50 resp. 6 as a function of temperature. For OFHC copper, i.e. with an RRR of 50, the electrical resistivity rises by 50 percents if going from zero field to 4.5 T. For phosphorous-deoxidized copper, the effect is much less dramatic, i.e. only 6 percents.

The thermal conductivity stays unchanged. In Figure 5, the thermal conductivity is plotted vs. temperature for both copper samples, i.e. an RRR of 50 and 6.

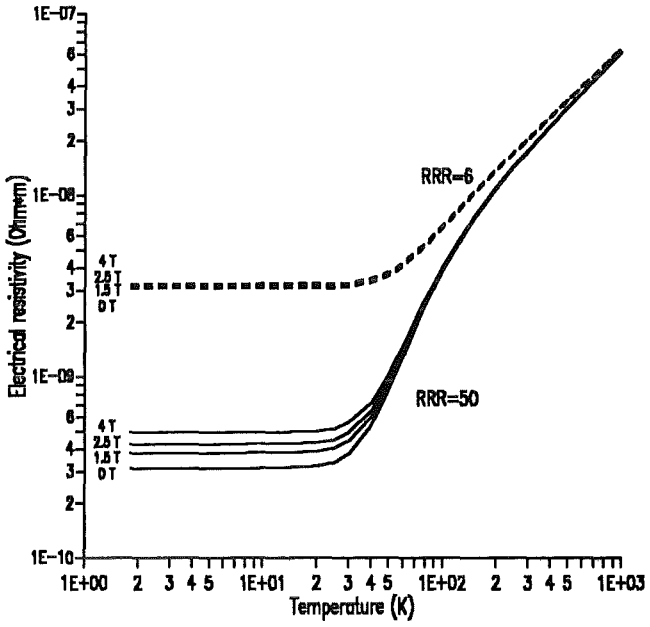

Figure 4. Electrical resistivity of copper vs. temperature: The full lines denote the values for an RRR of 50 whereas the dashed lines correspond to RRR of 6. The different lines of equal type denote different magnetic field values of zero, 1.5, 2.5, and 4 T

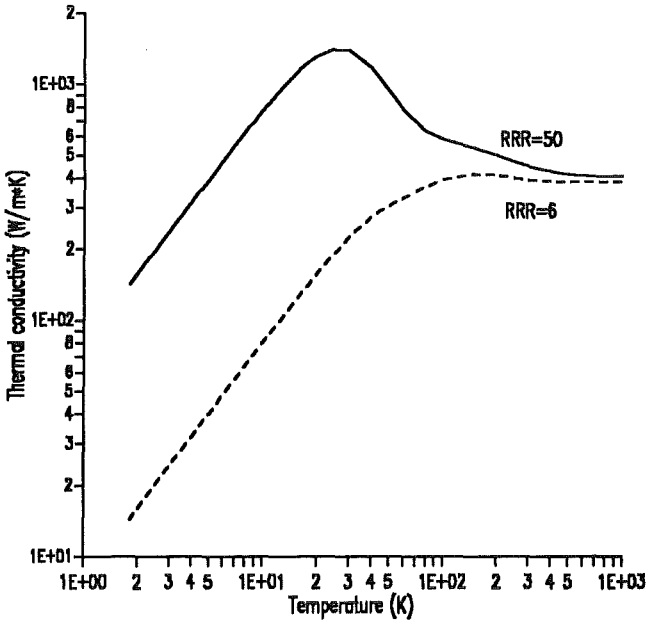

Figure 5. Thermal conductivity of copper vs. temperature: The full line denotes the values for an RRR of 50 whereas the dashed line corresponds to an RRR of 6

The effect of the new parameters for the superconductors given in Table 3 together with the higher electrical resistivity of the OFHC copper is exemplarily studied by computing the temperature distribution of the superconducting bus bar SCBUS once for zero magnetic field, and then for a constant magnetic field of 3.25 T which is roughly the average value over the location area. The geometrical data of the SCBUS are given in the next section and will not be quoted here. Figure 6 shows the resultant temperature profiles. For contact resistances of 10^{-9} Ω in both cases, there is no difference in the temperature profile if changing from zero field to 3.25 T because the maximum temperature in the copper is below the current sharing temperature of NbTi for both cases. The picture changes completely if computing the temperature profile for a contact resistance of 10^{-8} Ω. Now the maximum temperature is above the current sharing temperature of NbTi at 3.25 T which results in a completely overheating of the bus bar. Therefore one has to increase the helium mass flow rate from 2 g/s to 3.5 g/s. This result will be commented later.

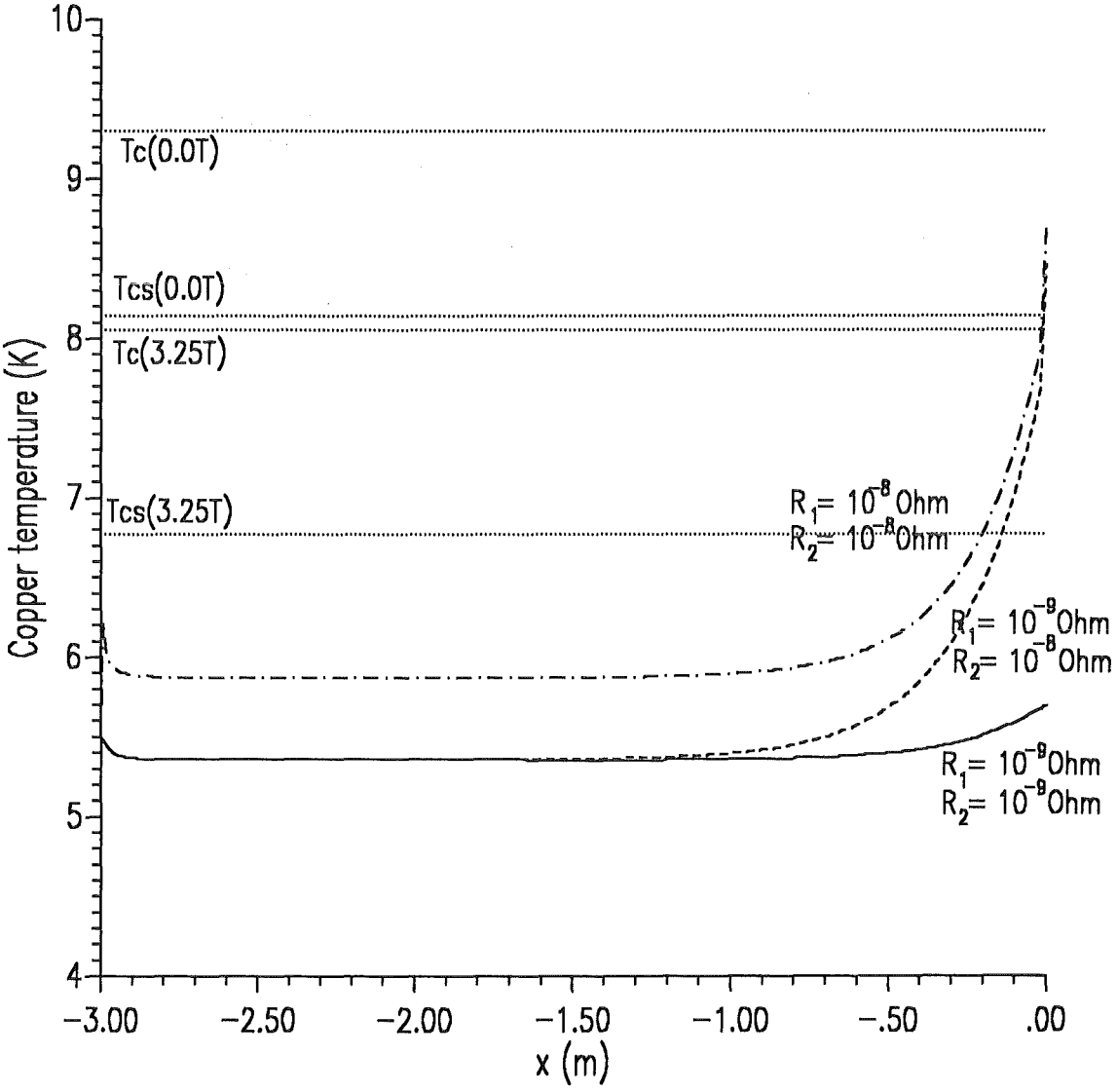

Figure 6. Temperature profile of the SCBUS for zero magnetic field: The dotted lines denote the current sharing resp. critical temperature of NbTi at 3.25 T and zero field

3.1.1 Temperature distributions for different contact resistances

The temperature profiles of the SCBUS were computed for different contact resistances by means of the computer code CURLEAD [9]

Due to the fact, that it is not possible to calculate two separated cooling circuits in CURLEAD simultaneously, the following procedure has been done:

1. The temperature profile has been calculated for three cases:
   - contact resistance between coil winding and bus bar $R_1 = 10^{-9}\ \Omega$, contact resistance between bus bar and current lead $R_2 = 10^{-9}\ \Omega$,
   - contact resistance between coil winding and bus bar $R_1 = 10^{-9}\ \Omega$, contact resistance between bus bar and current lead $R_2 = 10^{-8}\ \Omega$, and
   - contact resistance between coil winding and bus bar $R_1 = 10^{-8}\ \Omega$, contact resistance between bus bar and current lead $R_2 = 10^{-8}\ \Omega$.

   for different outlet conductor temperatures leading to different heat loads **out of the top end of the bus bar**. The assumption of having a negative slope of the temperature distribution at the top end is based on the fact that the cooling circuit of the current lead is able to cool the contact resistance R_2 additionally.
   Due to the different contact resistances, the design mass flow rates have to be changed, too. The increase of the contact resistance $R_2 = 10^{-9}\ \Omega$ be a factor of ten leads to an increase of the mass flow rate from 2 g/s to 3.25 g/s. This results in an increase of the negative slope at the bottom end of the superconducting bus bar, too.
2. The same was done for the current lead, i.e. the heat load from the bottom end of the heat exchanger was computed resulting from different copper temperatures at the bottom end. For this, the nominal helium mass flow rate has to be slightly modified correponding to [3] (from 2.77 g/s to 2.8 g/s).

The results are plotted in Figure 7. The intersection between the bus bar lines and the current lead line will give the connection temperature resp. heat load. For these numbers, the calculation was redone both for the bus bar and the current lead. Figure 8 shows the temperature profiles obtained for the superconducting bus bar whereas in Figure 9 the same is plotted for the superconducting bus bar together with the current lead. Again the effect of the different contact resistances is seen. In Table 4, the main results for the bus bar system as well as for the current lead are given.

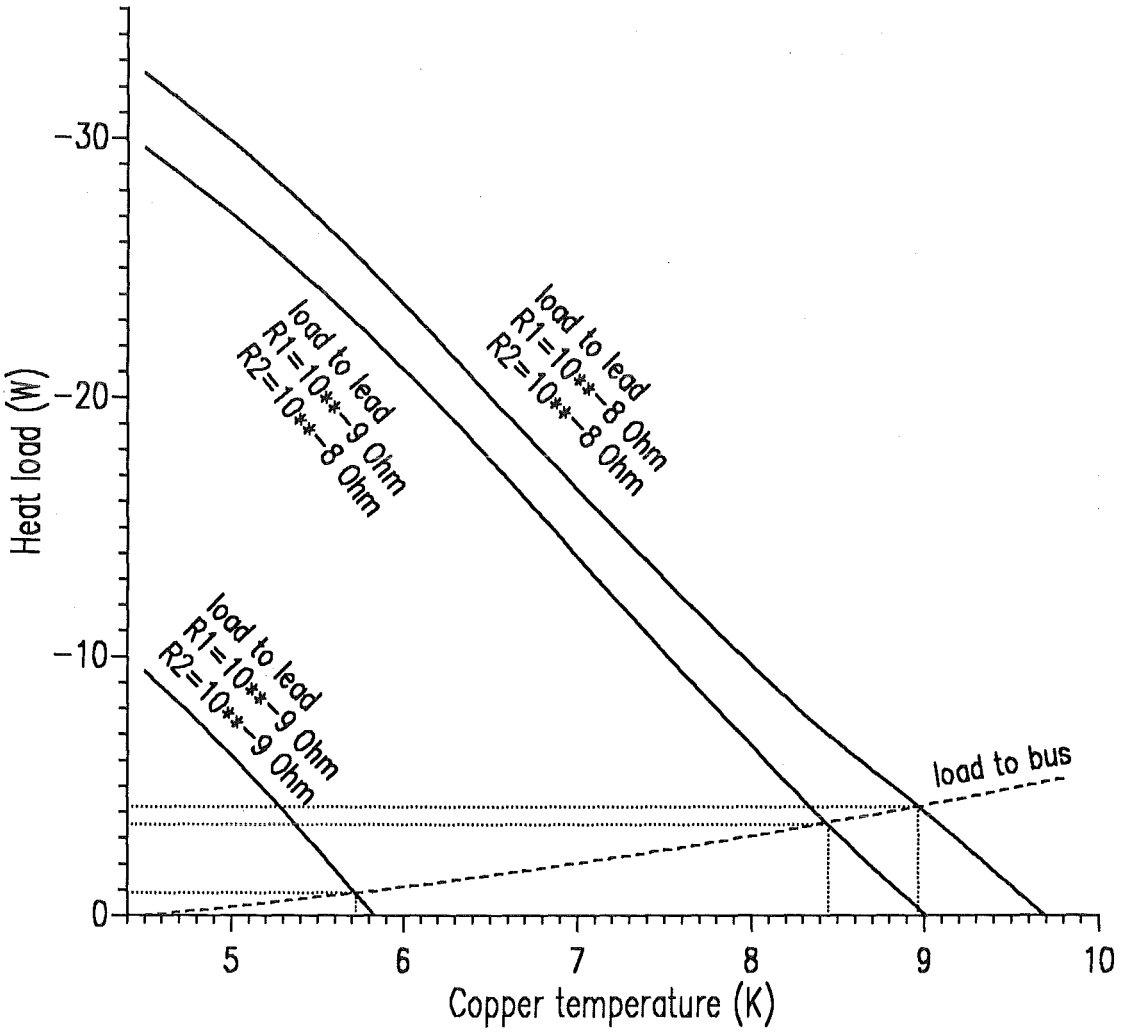

Figure 7. Heat load vs. outlet temperature of the conductor: The minus sign denotes the fact that the heat flows towards the current lead

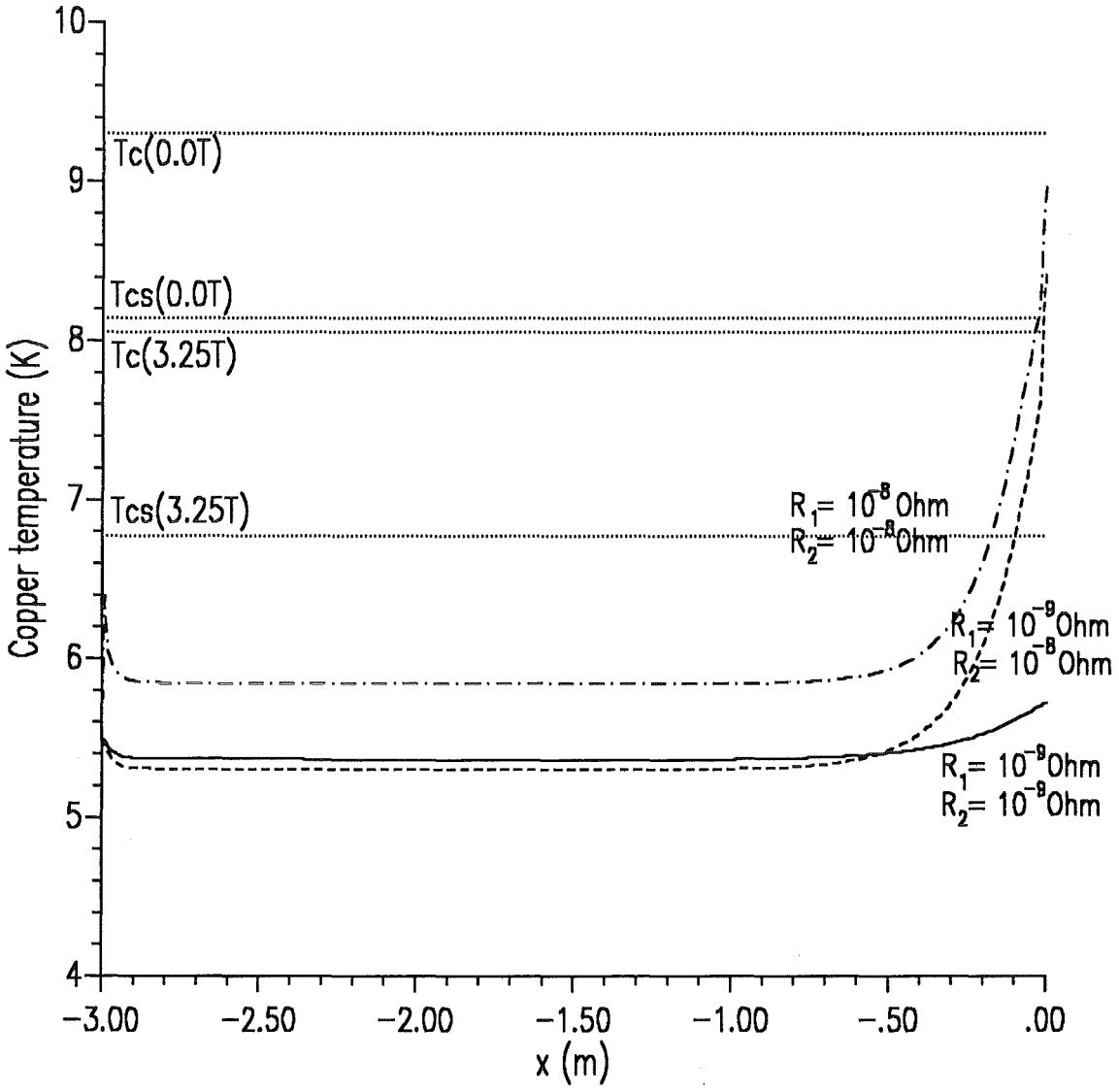

Figure 8. Temperature profiles of the conductor of the bus bar: The temperature distribution is shown for three different outlet temperatures of the conductor representing three different sets of contact resistances: the full line belongs to 10^{-9} Ω for both resistances, the dashed line to a contact resistance of 10^{-9} Ω for the coil bus bar connection and of 10^{-8} Ω for the bus bar lead connection, and the dash-dotted line corresponds to 10^{-8} Ω for both contact resistances

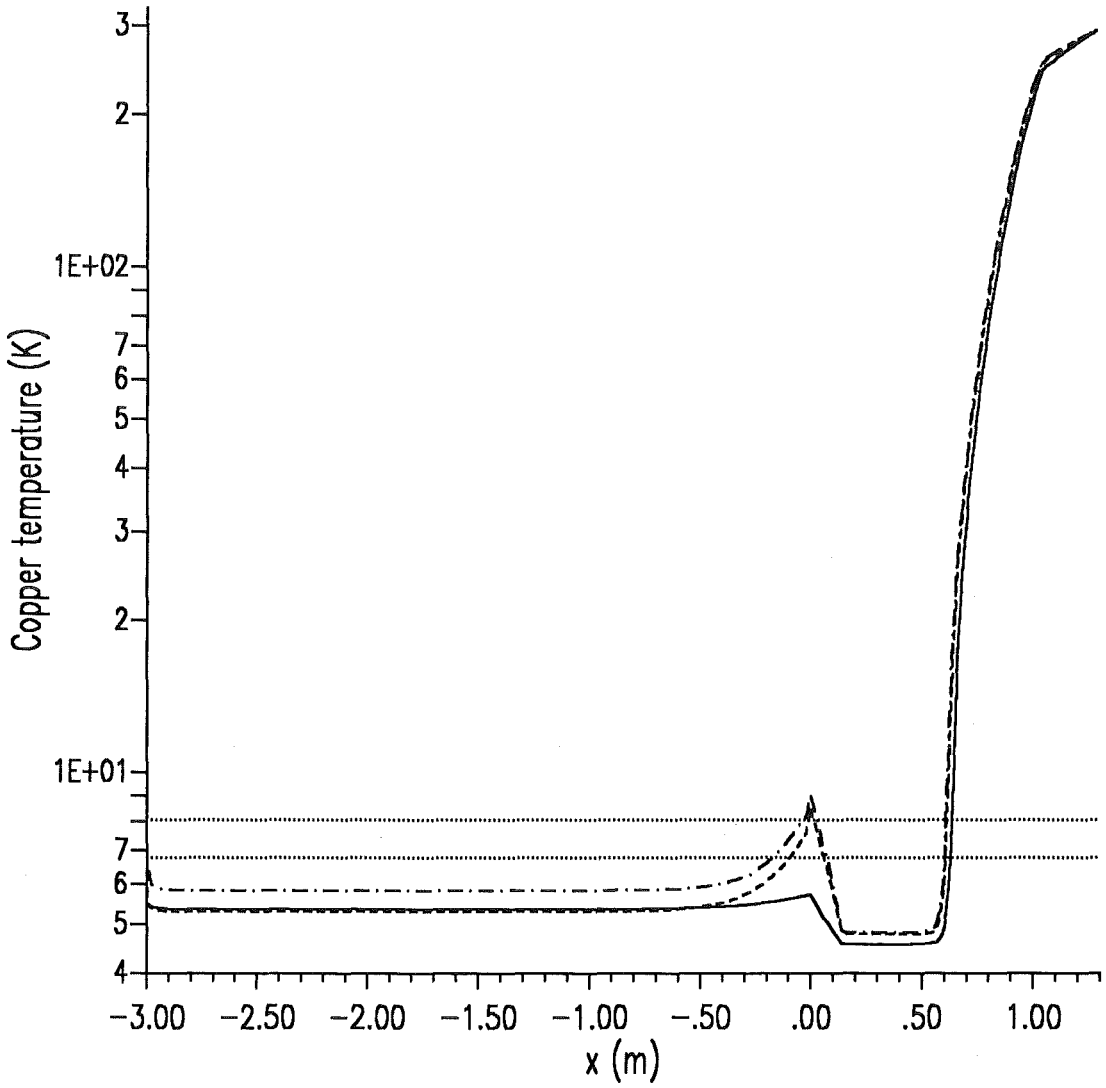

Figure 9. Temperature profiles of the conductor of the current lead and superconducting bus bar: The temperature distribution is shown for three different sets of contact resistances (as quoted for Figure 8)

R_1 R_2	$\dot{m}$	ΔU	Q_{bottom}	Q_{top}	$T_{top,Cu}$	$T_{top,He}$	$T_{max,Cu}$	$\dot{m}\,\Delta H$
[Ω]	[g/s]	[mV]	[W]	[W]	[K]	[K]	[K]	[W]
superconducting bus bar - SCBUS -								
10^{-9} 10^{-9}	2.0	0.20	-2.03	-0.79	5.72	5.67	5.72	10.07
10^{-9} 10^{-8}	3.25	1.38	-5.01	-3.53	8.44	7.23	8.53	53.28
10^{-8} 10^{-8}	3.5	2.42	23.16	-4.23	8.96	7.83	9.06	78.64
current lead								
10^{-9} 10^{-9}	2.8	68.42	-0.88	844.3	293.	291.9	293.	257.5
10^{-9} 10^{-8}	2.8	73.17	-3.58	611.9	293.	292.2	293.	257.5
10^{-8} 10^{-8}	2.8	74.46	-4.21	548.8	293.	292.3	293.	257.5

Table 4. Main results of the calculations of the temperature profile for the bus bar and the current lead: The calculations were done for three sets of contact resistances of the superconducting bus bar. The minus sign for the heat load at both ends of the SCBUS counts for the fact that the contact areas are cooled by the superconducting bus bar by heat conduction

The conclusion of the computations done so far is the following:

- The increase of the contact resistance either at the bus bar lead connection or at both ends lead to an increase of the maximum temperature of the conductor of the bus bar which is higher than the current sharing temperature of NbTi at least at zero field. The consequence is the necessity of increasing the helium mass flow rate from 2 g/s (case 1) to 3.5 g/s (case 3).
- Nevertheless, the maximum temperature of the conductor is above the current sharing temperature at 3.25 T. This leads additionally to an increase in the helium enthalpy difference, i.e. from 10 W (case 1) to about 80 W (case 3). The latter number is unacceptable with respect to the cooling capacity of the refrigerator.

The consequence is:
Contact resistances of about 10^{-9} Ω are an absolute requirement.

As a main result, only case 1 will be considered for the following studies, i.e. both contact resistances have values of 10^{-9} Ω.

In the following, different designs of a superconducting bus bar will be presented. For all alternatives, the steady state temperature distributions have been computed, the transient behaviour in case of loss of mass flow have been studied without and with energy dump of the model coils, and last the effect of AC losses during transient operations has been investigated.

4. Numerical results of steady state and transient calculations

4.1 General remarks

The behaviour of the superconducting bus bar under operating conditions as well as under fault conditions has been studied for five different types of superconducting bus bars:

- steady state temperature distribution at 50 kA with different contact resistances,
- transient behaviour, i.e. temperature distribution for
  - loss of cooling,
  - energy dump without taking into account the eddy current losses,
- eddy current losses in the stabilizing copper during energy dump

4.2 Superconducting bus bar system scaled from the 1.8 K test of the EURATOM LCT coil (SCBUS)

Starting from the superconducting bus bar designed for the 1.8 K test of the EURATOM LCT coil in TOSKA Upgrade, a first attempt was made for the design of a 50 kA bus bar. A schematic is shown in Figure 10. The superconducting bus bar consists of a central cable-in-conduit superconductor made of about 720 NbTi strands with a copper to non-copper ratio of 2.5 and an operating current of 50 kA which is half of the critical current of the superconductor at 3.3 T and 5.5 K. The critical temperature of NbTi was set in CURLEAD to 8.05 K, the current sharing temperature to 6.77 K. The amount of stabilizing copper which will be placed around the central superconductor has been obtained by scaling the superconducting bus bar of the LCT coil test in TOSKA from 10 kA to 50 kA in terms of ohmic power. It has to be guaranteed that there is a good electrical contact between the strands of the cable-in-conduit and the stabilizing copper profile. In the following, this type of bus bar is called SCBUS.

It should be noted that the total copper to superconductor ratio in the SCBUS is about 80.

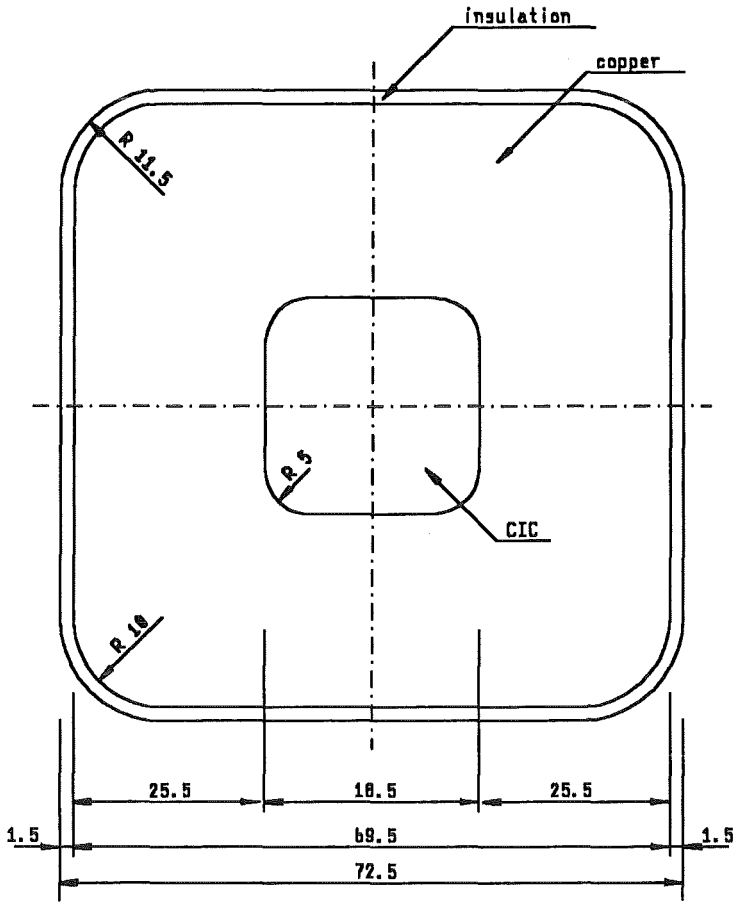

Figure 10. Transversal cross section of the superconducting bus bar SCBUS: Dimensions are in mm

Table 5 summarizes the geometrical numbers of the superconducting bus bar obtained by this procedure. These numbers have been used in the following. In Table 6, the wire data are given. It should be mentioned that the inlet temperature at the conductor of the superconducting bus bar of 5.5 K, i.e. a temperature difference of 1 K in the winding of the model coils has been arbitrarily chosen but so to be on the safe side because there is neither a design mass flow nor a design pressure.

Parameter of the SCBUS	Unit	Value
Length	m	3.0
RRR of copper stabilizer of s.c. bus		50
ρ(T=5.5K,B=0.0T,RRR=50)	Ωm	$3.2 \cdot 10^{-10}$
ρ(T=5.5K,B=3.5T,RRR=50)	Ωm	$4.9 \cdot 10^{-10}$
Outer dimensions of the cable-in-conduit (CIC)	mm x mm	18.5 x 18.5
Cross section of the CIC A_{CIC} (with rounded corners)	mm^2	321.01
Cross section of copper in CIC $A_{Cu\text{-}CIC}$	mm^2	137.575
Cross section of NbTi in CIC $A_{NbTi\text{-}CIC}$	mm^2	55.03
Cross section of helium in CIC $A_{He\text{-}CIC}$	mm^2	128.403
Cooled perimeter of strands P_{cool} (2/3 of strand perimeter)	mm	922.
Outer dimensions of the SCBUS (with insulation, rounded corners)	mm x mm	72.5 x 72.5
Outer dimensions of the SCBUS (without insulation, rounded corners)	mm x mm	69.5 x 69.5
Cross section of copper profile $A_{Cu\text{-}prf}$ (rounded corners)	mm^2	4560.976
Nominal current	kA	50
Nominal self field	T	1.08
Design helium pressure	bar	7.5
Design helium mass flow	g/s	2.0

Table 5. General data of the SCBUS

Parameter	Unit	Value
Strand diameter	mm	0.58
Number of strands		720 (30 x 6 x 4)
Wetted perimeter (2/3 of strand perimeter)	m	0.922
Helium inlet temperature	K	4.5
Strand non copper operational current density (4.5 K, 4.0 T)	A/mm^2	909
Copper area	mm^2	137.5
Superconductor area	mm^2	55.0
Helium area	mm^2	118.7
Void fraction	%	37
Copper : superconductor ratio, α		2.5
RRR of copper of wire		100
ρ(T=5.5K,B=3.5T,RRR=100)	Ωm	$3.2 \cdot 10^{-10}$
Cable space area	mm^2	320.8
Cable corner radii	mm	5
Cable aspect ratio		1 : 1
Conductor critical current (4.5 K, 4.0 T) (5.5 K, 4.0 T) (5.5 K, 5.6 T)	kA	 121.44 85.25 55.58

Table 6. General wire data of the SCBUS

The temperature distribution is plotted in Figure 9 in the last section.

4.3 Transient behaviour of the SCBUS

4.3.1 Loss of mass flow

The transient behaviour of the superconducting bus bar in case of a loss of helium mass flow has been studied for two different cases:

1. no energy dump of the coils
2. energy dump of the coil, i.e. exponential decay of the coil current with a dump time constant of $\tau_{dump} = 3$ s.

The temperature profile of the bus bar has been computed for different times after switching off the helium mass flow. In the calculations was assumed that the heat load towards the coil will be zero whereas the heat load towards the current lead will stay at the steady state value of -0.79 W.

Figure 11 shows the resultant temperature profiles up to 60 s after switching off the mass flow. For clarity, a logarithmic scale has been chosen. The result is that the loss of helium mass flow in case of no energy dump leads to a quench of the superconducting bus bar after 20 s due to the high power input which can neither be transferred to the helium cooling nor towards the ends by

heat conduction. The quench will start at the region near to the coil. The maximum temperature in the conductor after 60 s is about 30 K but it will continue to rise.

A characteristic for all kind of superconducting bus bars reported here is that in case of loss of helium mass flow the heating starts at the connection which is near the coil and propagates in both directions leading to a more homogeneous temperature rise along the conductor.

In contradicton, in case of an energy dump, there is no increase of temperature within 20 s which is more than six times the dump time constant of 3 s. The corresponding temperature profiles have been plotted in Figure 12. Here, a linear scale has been used. Moreover, the temperatures decrease because the power input is reduced during dump.

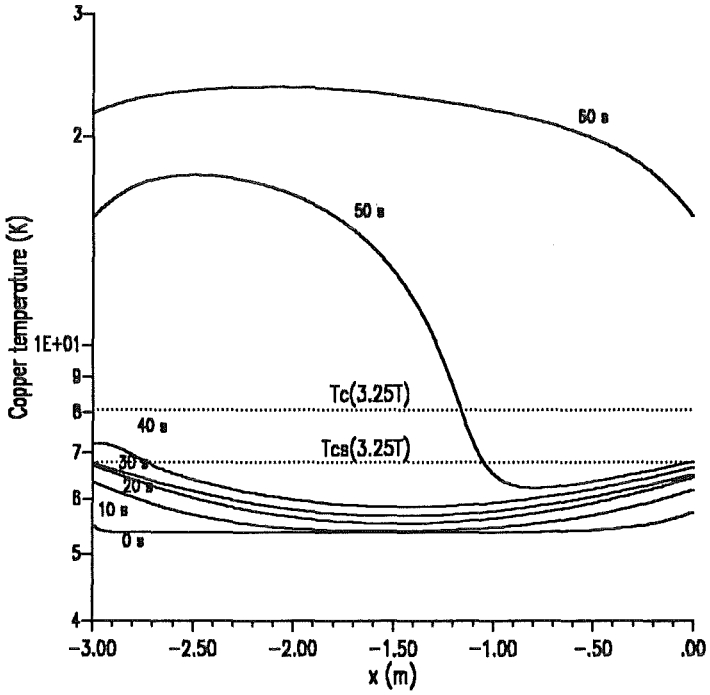

Figure 11. **Temperature profiles of the conductor of the SCBUS for different times after switching off the mass flow without energy dump**

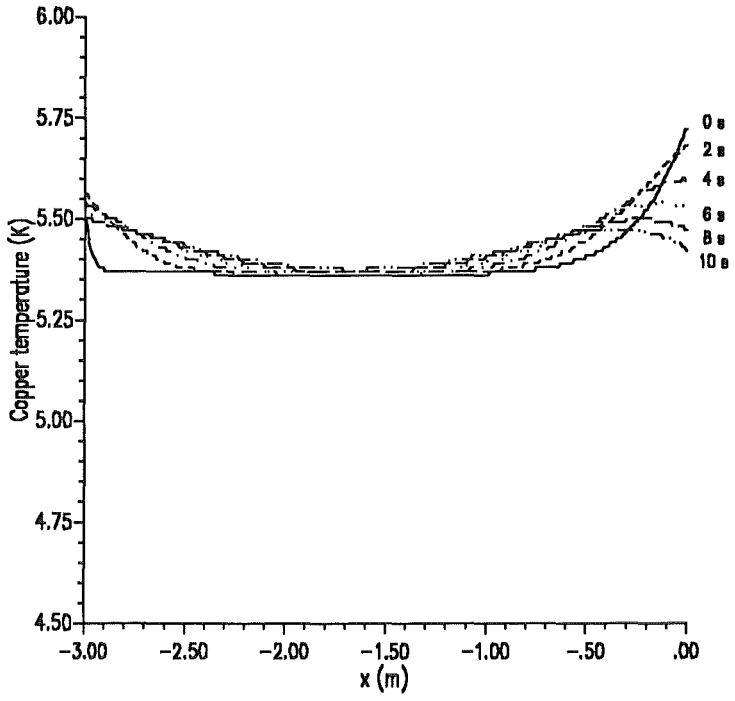

Figure 12. **Temperature profiles of the conductor of the SCBUS for different times after switching off the mass flow with energy dump:** A dump time constant of 3 s has been used

4.3.2 Eddy current losses during energy dump

Up to now, it was assumed that during a fast discharge of the coil stack, i.e. a decay of the coil current with a time constant of 3 s there is no additional power input. But this is not true because a fast discharge of the coils will be accomplished by a fast change of the magnetic field also at the location area of the superconducting bus bar. This will lead to AC-losses, i.e.

1. hysteresis losses in the superconducting filaments of the CIC,
2. coupling losses in the copper matrix of the CIC, and
3. eddy current losses in the copper stabilizer profile.

The last item should yield the most important contribution to the total AC-losses. Due to this, calculations will be presented here based on analytic expressions presented in section 2. These formulas are expressed in terms of energy density resp. energy per unit length if taking into account the conductor cross section. In Table 7 the geometric numbers which enter the analytic expressions are summarized.

The transversal resistivity in a subcable resp. between them is not well determined. Measurements, e.g. by ABB, resulted in resistivities in the order of 10^{-8} to 10^{-7} Ωm. Therefore ABB used in its study an average value of $5 \cdot 10^{-8}$ Ωm [10]. This number has been used in the calculations, too.

Parameter	Unit	Value
Hysteresis losses		
Filament diameter d	mm	0.0447
λ		0.286
Critical current density j_c (at 3.6 T, 5.5 K) (at 2.0 T, 5.5 K)	 A/mm² A/mm²	 1690. 2256.
Coupling losses		
Filament twist pitch l_f	mm	10
Twist pitch of first stage $l_{p,1}$ (estimation)	mm	25
Twist pitch of second stage $l_{p,2}$ (estimation)	mm	100
Twist pitch of third stage $l_{p,2}$ (estimation)	mm	300
Number of wires in subcable		30
Number of subcables in stage 2		6
Number of subcables in stage 3		4
Resistivity of matrix ρ_{matrix} (Cu (RRR = 100 at 3.6 T, 5.5 K)) (Cu (RRR = 100 at 2.0 T, 5.5 K))	 Ωm Ωm	 $3.2 \cdot 10^{-10}$ $2.5 \cdot 10^{-10}$
Resistivity of subcable resp. cable	Ωm	$5 \cdot 10^{-8}$
Eddy current losses		
A_{jacket}/A_{wire}		23.17385
Outer length of jacket a resp. b	mm	69.5
Inner length of jacket c resp. d	mm	18.5
Jacket resistivity ρ (Cu (RRR = 50 at 3.6 T, 5.5 K)) (Cu (RRR = 50 at 2.0 T, 5.5 K))	 Ωm Ωm	 $4.8 \cdot 10^{-10}$ $4.1 \cdot 10^{-10}$

Table 7. Geometrical input data for AC-loss calculation of the SCBUS

In Table 8, the computed values for the integrals expressed above are given in case of an energy dump of the model coils. A dump time constant of 3 s has been used. The magnetic field values at the location of the superconducting bus bar resp. the current lead are due to the field of the model coil stack. The self-field of the bus bar resp. current lead (only transverse direction) has to be added to get the final values.

Position	Value					
	transversal			parallel		
	B_{abs}	$\int \dot{B}\,dt$	$\int \dot{B}^2\,dt$	B_{abs}	$\int \dot{B}\,dt$	$\int \dot{B}^2\,dt$
	T	T	T^2/s	T	T	T^2/s
Model coil (position of maximum field)	13.5	13.5	30.4	0	0	0
Superconducting bus	3.58	3.58	2.14	2.0	2.0	0.67

Table 8. Integral magnetic field changes at the positions of the inner model coils, the superconducting bus bar resp. current lead in case of an energy dump

Table 9 shows the coupling time constants resp. the resultant AC losses. Here, the magnetic field changes given in Table 8 are used.

Parameter	Unit	Transversal	Parallel
Hysteresis losses	mJ/cm^3	16.40	3.06
Coupling losses: composite 1. cable stage 2. cable stage 3. cable stage	mJ/cm^3	 15.33 0.17 2.65 23.67	 6.10 0.11 1.71 15.25
Eddy current losses in the jacket	mJ/cm^3	44535.23	8160.86
Sum	mJ/cm^3 J/m	44593. 8589.	8187. 1577.
Total losses	W/m	954	175

Table 9. Average AC-losses in the SCBUS due to an exponential energy dump of the model coils

It should be mentioned that the analytic expression used for calculating the eddy current losses in the copper stabilizer profile is not very accurate. Therefore, the result is only an estimation, and more detailed calculations would be necessary to get a better result. Unfortunately, these kind of losses are by far the dominant ones. As measurements for the EURATOM-LCT coil in the ISMTF facility at Oak Ridge showed, that the calculations done for the LCT coil casing by using the formula for the eddy current losses result in values which are a factor of two too high. Therefore, for the further analysis, the total losses were divided by two to look on the transient behaviour.

The equivalent values for plasma disruption expected for the toroidal field coils in NET/ITER are

$$\int_0^{100ms} \dot{B}\,dt = 1T$$

resp.

$$\int_0^{100ms} \dot{B}^2 dt = 10T^2/s$$

If the same integral field changes would be valid for the bus bar, the coupling losses resp. eddy current losses will be a factor of 10 higher than in case of an energy dump in TOSKA Upgrade whereas the hysteresis losses will be a factor of 2 lower. Because the eddy current losses are the dominant contributor to the AC-losses, the total losses will be one order of magnitude higher in case of a plasma disruption simulation.

In fact, the NET/ITER requirements are not so urgent because the inner part of the tokamak (blanket, first wall) resp. the toroidal field coils absorb most of the energy of the plasma disruption. In addition, the magnetic field at the location of the bus bar will be lower than at the inner radius of the coil, i.e. the magnetic field change will be less dramatic.

The computer code CURLEAD has been modified in such a way that it is now possible to add an external heat source in terms of power per unit length. So the temperature rise due to this additional heat input could be calculated.

Starting from the steady state solution of the temperature profile of the superconducting bus bar for a mass flow rate of 2 g/s, an energy dump of the coil stack with a continuous helium mass flow through the bus bar of 2 g/s and an external heat of 600 W/m has been computed for different times. Figure 13 shows the results.

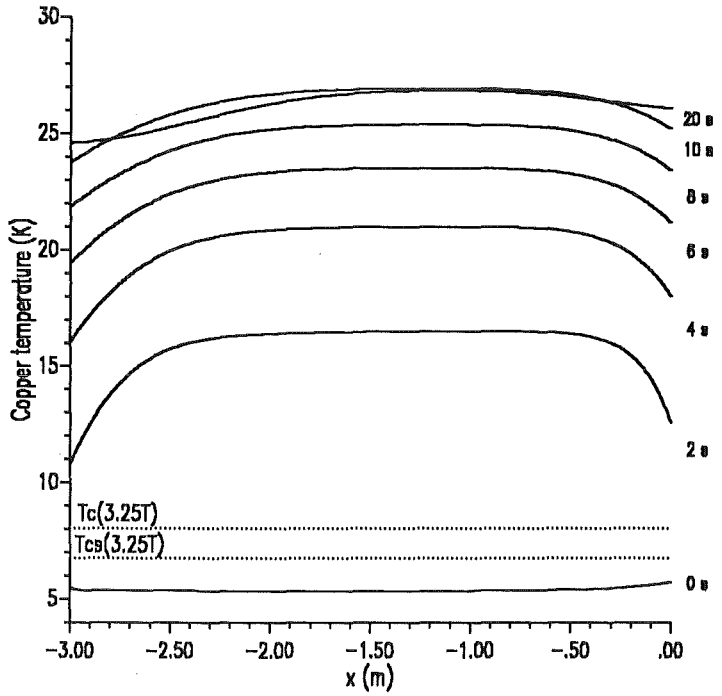

Figure 13. Temperature profiles of the conductor of the SCBUS for different times after starting the energy dump including a heat input of 600 W/m: A dump time constant of 3 s has been used

The result is that the external heat input is so high that the helium mass flow rate is not able to transfer the heat. This can be also concluded from a simple energy balance: for a cooling perimeter of roughly 90 cm and a mean heat transfer coefficient of 350 W/m^2K one gets a temperature difference of about 1.8 K. This means that the maximum temperature in the conductor of the bus bar rises from 5.7 K to 7.5 K, i.e. already above the current sharing temperature of NbTi. But the enthalpy difference of the helium for a mass flow rate of 2 g/s (11 W) is much too low to pick up

the offered heat (1.7 kW). The superconducting bus bar must quench due to this enormously high heat input.

The conclusion is that one has to reduce the AC-losses by more than two orders of magnitude.

To do this, two possiblities can be investigated:

- If the amount of copper is needed to prevent the superconducting bus bar against overheating one has to rearrange the material substrats.
- If the high energy input has to be withstood one has to reduce the stabilizing copper part drastically.

4.4 Modification of the SCBUS - copper nickel coated copper wire stabilizer (CONIBUS)

An interesting alternative for a large stabilizer with low eddy current losses had been proposed by PSI for their NET toroidal field conductor design [11]. They started from copper wires of about 1 mm diameter with a thin copper-nickel coating of about 130 μ. The wires were twisted with a twist length of about 1 m and afterwards hardly pressed to get a rigid profile. The aim was to enlarge the resistivity against eddy currents generated by tansverse magnetic field changes. This type of bus bar is called CONIBUS.

In our case, the copper stabilizer is divided into four subparts. For each subpart, about 180 wires are needed, and a twist pitch of 500 mm is assumed whereas the diameter of the copper wires resp. the thickness of the copper-nickel coating are the same. The eddy current losses in the honeycomb-like stabilizer are calculated by computing the effective resistivity using the formula given in [12].

Transversal:

$$\rho_e = \frac{\rho_c \cdot d_c}{d_c + d_n} + \rho_n \cdot \frac{d_n}{d_c + d_n} \cdot \sin\theta$$

where
ρ_c = resistivity of copper (ρ(3.6 T, 5.5 K) = $4.8 \cdot 10^{-10}$ Ωm),
ρ_n = resistivity of copper-nickel (ρ = $1.4 \cdot 10^{-7}$ Ωm),
d_c = thickness of copper in one cell,
d_n = thickness of copper-nickel in one cell, and
θ = twist angle of stabilizer.
This results in a transversal effective resistivity of $1.26 \cdot 10^{-9}$ Ωm

Longitudinal:
[6] uses an effective resistivity for longitudinal field variation of $6 \cdot 10^{-9}$ Ωm.

Using the numbers given above this results in an averaged transversal time constant of 108 ms resp. a longitudinal time constant of 7 ms. Table 10 summarizes the AC-losses obtained.

Parameter	Unit	Transversal	Parallel
Hysteresis losses	mJ/cm^3	16.40	3.06
Coupling losses: composite 1. cable stage 2. cable stage 3. cable stage	mJ/cm^3	 15.33 0.17 2.65 23.67	 6.10 0.11 1.71 15.25
Eddy current losses in the jacket	mJ/cm^3	4262.17	86.49
Sum	mJ/cm^3 J/m	7320. 832.	113. 22.
Total losses	W/m	93.	3.

Table 10. Average AC-losses in the CONIBUS due to an exponential energy dump of the model coils

The conclusion is the transversal losses are reduced by a factor of twelve. But besides the difficulty in the production of such a copper stabilizer, the losses are too high.

4.5 Modification of the SCBUS - reduced copper stabilizing bus (LCOBUS)

One possibility to overcome the problem of quenching is to reduce the amount of stabilizing copper around the CIC. For the calculations presented in this section a copper to non-copper ratio of 15 has been assumed instead of 80 in the last section. This results in a much reduced copper profile although the design base has been unchanged. This type of bus bar is called LCOBUS.

Now, the outer length of the superconducting bus bar will be 33.1 mm (instead of 69.5 mm) whereas the outer length of the CIC in the bus bar will stay fixed at 18.5 mm.

The temperature profile of the bus bar has been computed by means of CURLEAD only with contact resistances of 10^{-9} Ω. Figure 14 shows the resultant temperature distribution, for comparison the one of the highly stabilized bus bar has been shown, too. The difference is mainly in the lower temperature level along the bus bar leading to a smaller heat load towards the coil end. The reason is the lower heat conduction due to the smaller copper cross section.

Table 11 summarizes the computational results of the temperature profile calculations. For comparison, the results of the SCBUS are also given.

R_1 R_2	$\dot{m}$	ΔU	Q_{bottom}	Q_{top}	$T_{top,Cu}$	$T_{top,He}$	$T_{max,Cu}$	$\dot{m}\,\Delta H$
[Ω]	[g/s]	[mV]	[W]	[W]	[K]	[K]	[K]	[W]
superconducting bus bar ($\alpha = 80$) - SCBUS -								
10^{-9} 10^{-9}	2.0	0.20	-2.03	-0.79	5.72	5.67	5.72	10.07
superconducting bus bar ($\alpha = 15$) - LCOBUS -								
10^{-9} 10^{-9}	2.0	0.20	-0.42	-1.05	5.66	5.48	5.66	8.25

Table 11. Main results of the calculations of the temperature profile for the LCOBUS: The minus sign for the heat load at both ends of the LCOBUS counts for the fact that the contact areas are cooled by the superconducting bus bar by heat conduction

The behaviour of the LCOBUS in case of loss of mass flow has been simulated in the same way as for the SCBUS, i.e. without energy dump and with an exponential current decay with a time constant of 3 s. Figure 15 and Figure 16 show the resultant temperature profiles along the length with time as parameter. The result is that the LCOBUS has a lower safety margin in case of a loss of mass flow and no consecutive energy dump than the highly stabilized one. Note that in Figure 15, the temperature scale is different from that in Figure 11.

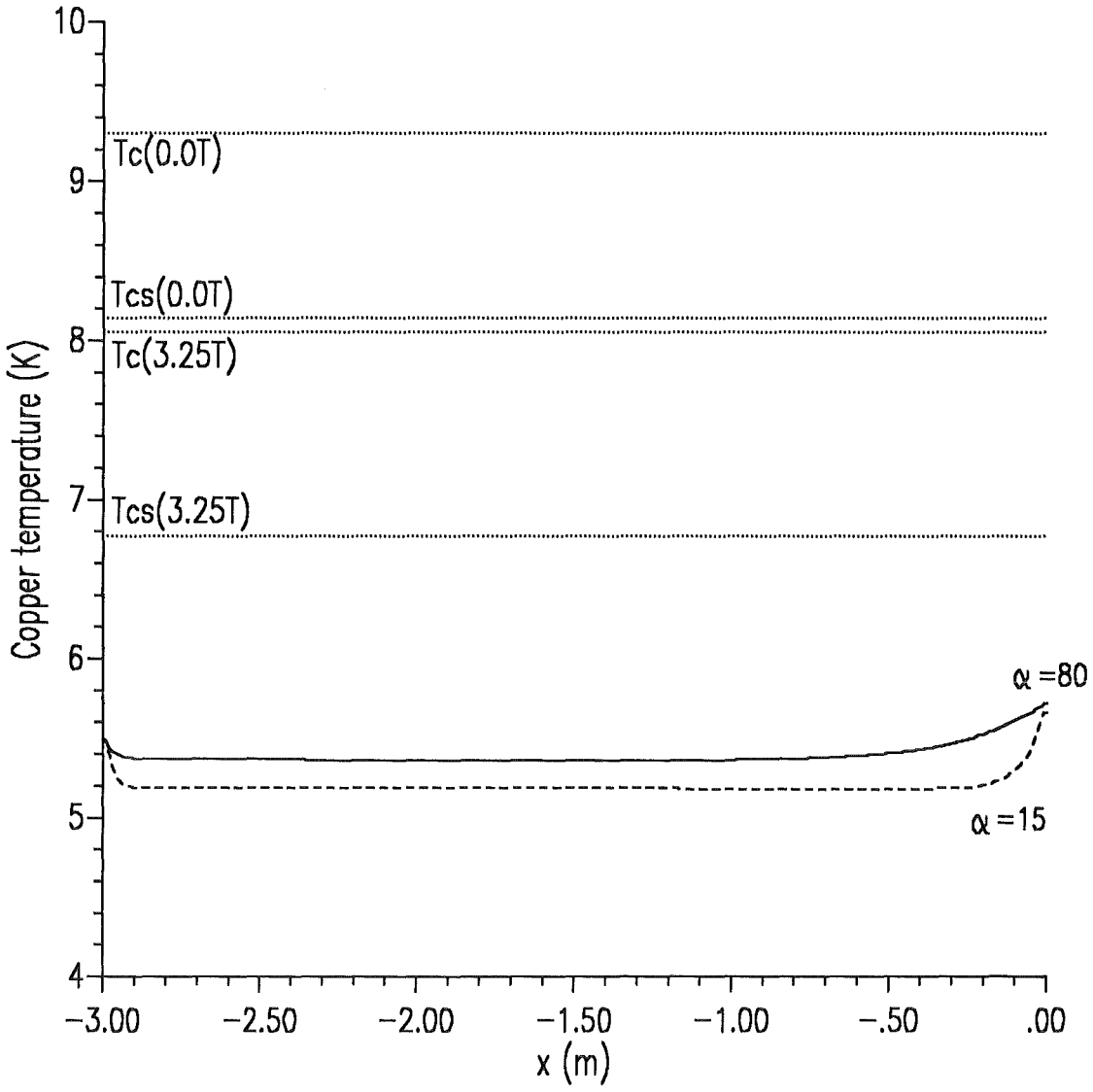

Figure 14. Temperature profile of the conductor of the LCOBUS: The related profile has been plotted as a full line whereas the dotted line corresponds to the SCBUS discussed in the last chapter.

Now the AC-losses induced in the superconducting bus bar were computed again in the same way as for the SCBUS. Table 12 summarizes the geometrical data of the low copper bus bar (LCOBUS) whereas is Table 13 the AC-losses have been collected.

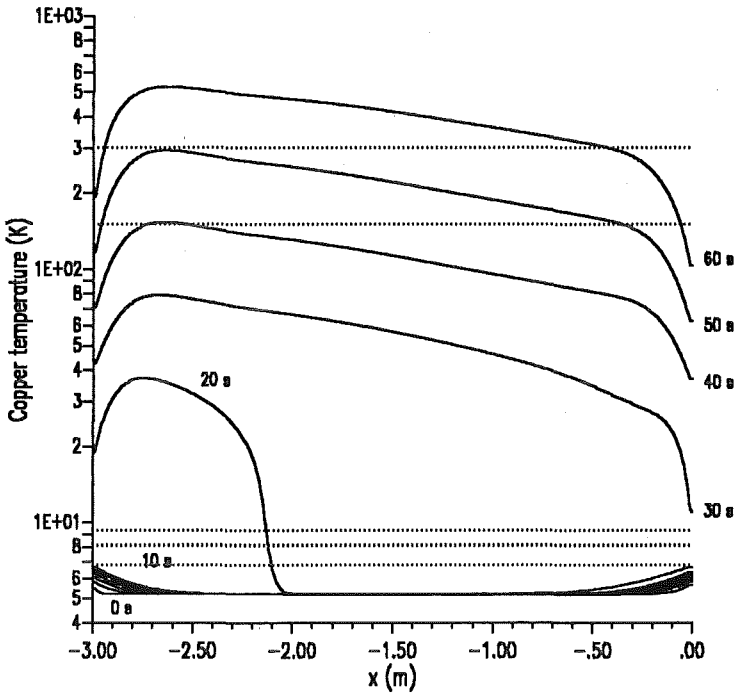

Figure 15. Temperature profiles of the conductor of the LCOBUS for different times after switching off the mass flow without energy dump

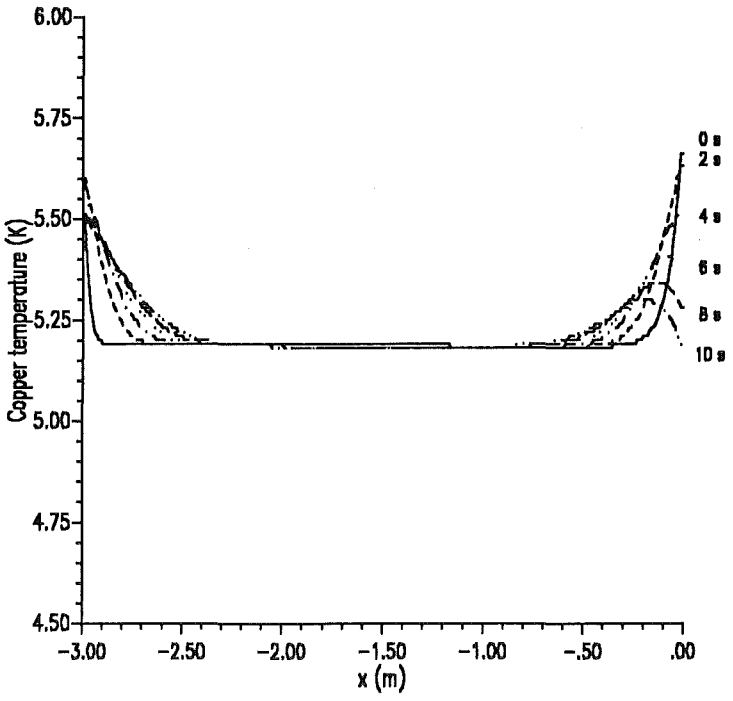

Figure 16. Temperature profiles of the conductor of the LCOBUS for different times after switching off the mass flow with energy dump: A dump time constant of 3 s has been used

Parameter	Unit	Value
Hysteresis losses		
Filament diameter d	mm	0.0447
λ		0.286
Critical current density j_c (at 3.6 T, 5.5 K) (at 2.0 T, 5.5 K)	 A/mm^2 A/mm^2	 1690. 2256.
Coupling losses		
Filament twist pitch l_f	mm	10
Twist pitch of first stage $l_{p,1}$ (estimation)	mm	25
Twist pitch of second stage $l_{p,2}$ (estimation)	mm	100
Twist pitch of third stage $l_{p,2}$ (estimation)	mm	300
Number of wires in subcable		30
Number of subcables in stage 2		6
Number of subcables in stage 3		4
Twist angle θ	°	3
Resistivity of matrix ρ_{matrix} (Cu (RRR = 100 at 3.6 T, 5.5 K)) (Cu (RRR = 100 at 2.0 T, 5.5 K))	 Ωm Ωm	 $3.2 \cdot 10^{-10}$ $2.5 \cdot 10^{-10}$
Resistivity of subcable resp. cable	Ωm	$5 \cdot 10^{-8}$
Eddy current losses		
A_{jacket}/A_{wire}		2.14286
Outer length of jacket a resp. b	mm	33.1
Inner length of jacket c resp. d	mm	18.5
Jacket resistivity ρ (Cu (RRR = 50 at 3.6 T, 5.5 K)) (Cu (RRR = 50 at 2.0 T, 5.5 K))	 Ωm Ωm	 $4.8 \cdot 10^{-10}$ $4.1 \cdot 10^{-10}$

Table 12. Geometrical input data for AC-loss calculation of the LCOBUS

Parameter	Unit	Transversal	Parallel
Hysteresis losses	mJ/cm^3	16.40	3.06
Coupling losses: composite 1. cable stage 2. cable stage 3. cable stage	mJ/cm^3	 15.33 0.17 2.65 23.67	 6.10 0.11 1.71 15.25
Eddy current losses in the jacket	mJ/cm^3	1146.	209.7
Sum	mJ/cm^3 J/m	1204. 232.	237. 46.
Total losses	W/m	26	5.1

Table 13. Average AC-losses in the LCOBUS due to an exponential energy dump of the model coils

Due to the same reason as in the section before, the total losses were divided by two to look on the transient behaviour.

The temperature profiles of the bus bar during loss of mass flow and a consecutive dump with a time constant of 3 s have been calculated for different times while an external heat of 20 W/m has been put onto the conductor. CURLEAD computes the temperature distributions by assuming no heat load towards the coil and a constant heat load of 0.83 W towards the lead. In Figure 17 the temperature distributions are shown for different times after starting the energy dump of the coil and a continuous mass flow through the bus bar. The maximum temperature after 10 s (three times the dump time constant) is about 7.5 K, i.e. the maximum temperature is already in the current sharing region of the NbTi superconductor. After further 10 s, the LCOBUS has a lower temperature, i.e. recovery is possible.

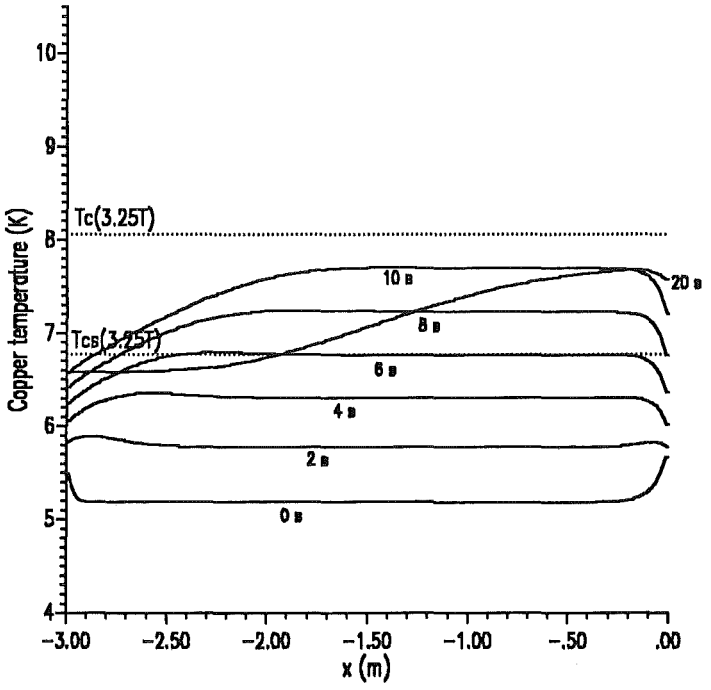

Figure 17. Temperature profiles of the conductor of the LCOBUS for different times after starting the energy dump including an external heat input of 20 W/m: A dump time constant of 3 s has been used

4.6 *A superconducting bus bar with no copper stabilizer (CICBUS)*

At fourth, the stabilizing copper profile has been removed completely, and was replaced by a jacket made of stainless steel with a thickness of 3 mm. In the following, this type of bus bar is called CICBUS.

At first, the temperature profile of the bus bar has been computed, again for contact resistivities of 10^{-9} Ω, as helium mass flow rate of 2 g/s, and a nominal current of 50 kA. Figure 18 shows the profile. For comparison, the temperature profile of the bus bars of the last sections have been plotted, too. Table 14 shows the computational results of the temperature profile calculations. For comparison, the results for the SCBUS and the LCOBUS have been added.

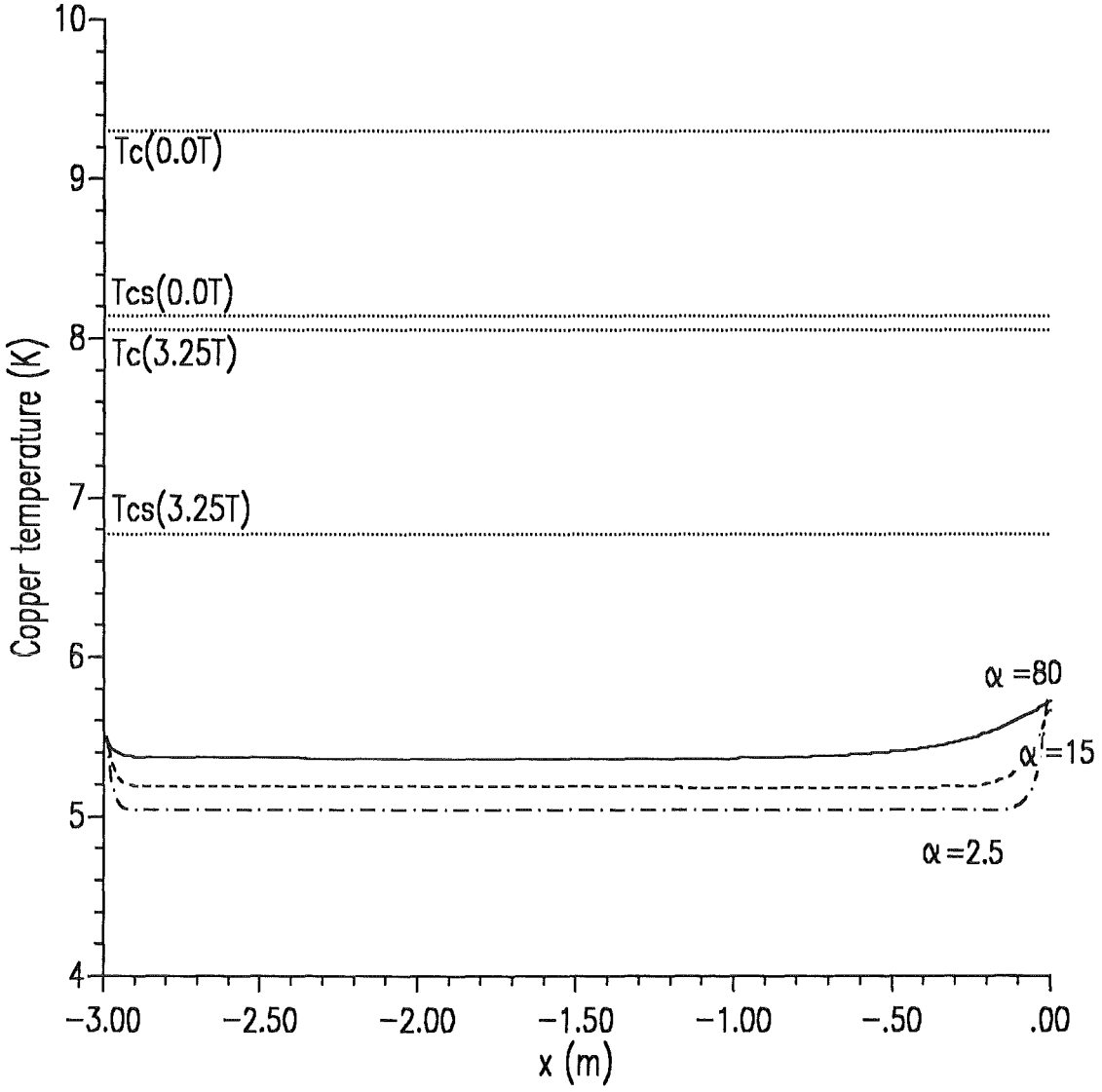

Figure 18. Temperature profile of the conductor of the CICBUS: The related profile has been plotted as a full line whereas the dotted line corresponds to the SCBUS and the dash-dotted line corresponds to the LOCUBUS

R_1 R_2	$\dot{m}$	ΔU	Q_{bottom}	Q_{top}	$T_{top,Cu}$	$T_{top,He}$	$T_{max,Cu}$	$\dot{m}\,\Delta H$
[Ω]	[g/s]	[mV]	[W]	[W]	[K]	[K]	[K]	[W]
superconducting bus bar ($\alpha = 80$) - SCBUS -								
10^{-9} 10^{-9}	2.0	0.20	-2.03	-0.79	5.72	5.67	5.72	10.07
superconducting bus bar ($\alpha = 2.5$) - CICBUS -								
10^{-9} 10^{-9}	2.0	0.20	0.86	-0.91	5.76	5.36	5.76	7.11

Table 14. Main results of the calculations of the temperature profile for the CICBUS: The minus sign for the heat load at both ends of the CICBUS counts for the fact that the contact areas are cooled by the superconducting bus bar by heat conduction

The behaviour of the CICBUS in case of loss of mass flow has been simulated in the same way as for the SCBUS and the LCOBUS, i.e. without energy dump and with an exponential current decay with a time constant of 3 s. Figure 19 and Figure 20 show the resultant temperature profiles along the length with time as parameter. Tes result is that the non-stabilized bus bar has a very low safety margin in case of a loss of mass flow if no energy dump will be initiated. The "camel"-like behaviour of the temperature profile is due to the fact that the copper cross section is drastically reduced leading to a higher electrical resistance and a lower thermal conductance, i.e. the Joule heat generated is higher and is not able to flow fast to neighbouring copper sections.

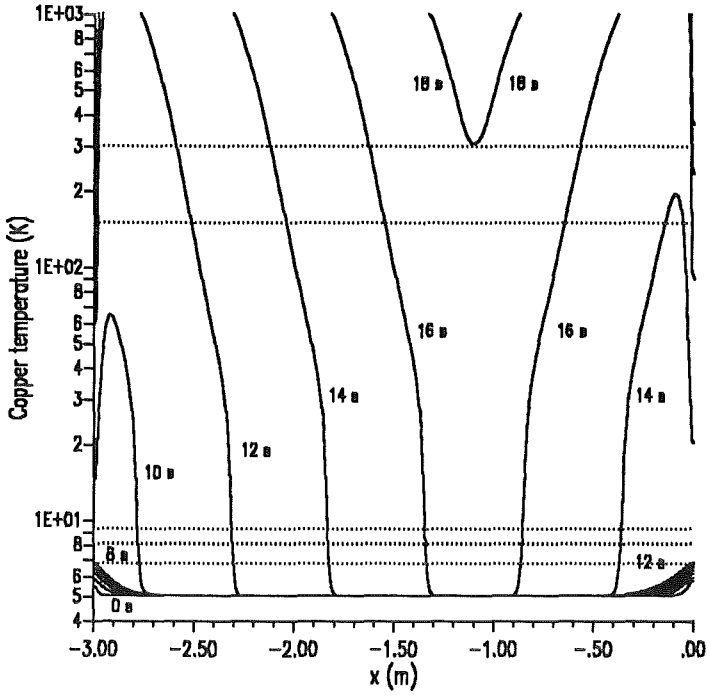

Figure 19. Temperature profiles of the conductor of the CICBUS for different times after switching off the mass flow without energy dump

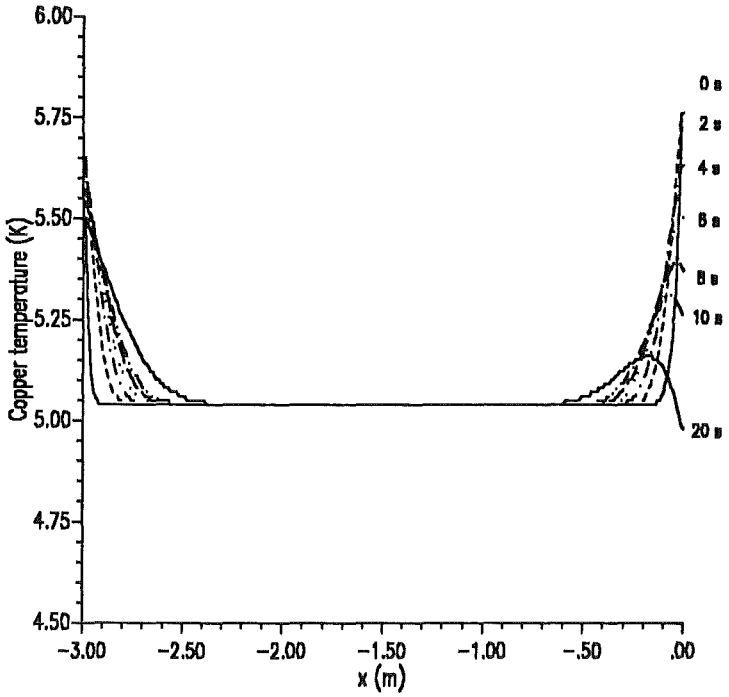

Figure 20. Temperature profiles of the conductor of the CICBUS for different times after switching off the mass flow with energy dump: A dump time constant of 3 s has been used

Now the AC-losses induced in the superconducting bus bar have been computed. Table 15 summarizes the input data for the AC-loss calculations whereas in Table 16 the resultant specific losses are presented.

Parameter	Unit	Value
Hysteresis losses		
Filament diameter d	mm	0.0447
λ		0.286
Critical current density j_c (at 3.6 T, 5.5 K) (at 2.0 T, 5.5 K)	 A/mm^2 A/mm^2	 1690. 2256.
Coupling losses		
Filament twist pitch l_f	mm	10
Twist pitch of first stage $l_{p,1}$ (estimation)	mm	25
Twist pitch of second stage $l_{p,2}$ (estimation)	mm	100
Twist pitch of third stage $l_{p,2}$ (estimation)	mm	300
Number of wires in subcable		30
Number of subcables in stage 2		6
Number of subcables in stage 3		4
Resistivity of matrix ρ_{matrix} (Cu (RRR = 100 at 3.6 T, 5.5 K)) (Cu (RRR = 100 at 2.0 T, 5.5 K))	 Ωm Ωm	 $3.2 \cdot 10^{-10}$ $2.5 \cdot 10^{-10}$
Resistivity of subcable resp. cable	Ωm	$5 \cdot 10^{-8}$
Eddy current losses		
A_{jacket}/A_{wire}		0.804265
Outer length of jacket a resp. b	mm	24.5
Inner length of jacket c resp. d	mm	18.5
Jacket resistivity ρ (stainless steel)	Ωm	$5.3 \cdot 10^{-7}$

Table 15. Geometrical input data for AC-loss calculation of the CICBUS

Parameter	Unit	Transversal	Parallel
Hysteresis losses	mJ/cm³	16.40	3.06
Coupling losses: composite 1. cable stage 2. cable stage 3. cable stage	mJ/cm³	 15.33 0.17 2.65 23.67	 6.1 0.11 1.71 15.25
Eddy current losses in the jacket	mJ/cm³	0.43	0.03
Sum	mJ/cm³ J/m	58.7 11.3	26.3 5.1
Total losses	W/m	1.3	0.6

Table 16. Average AC-losses in the CICBUS due to an exponential energy dump of the model coils

Figure 21 shows the temperature profile along the superconducting bus bar for different times after starting the energy dump which generates the AC-losses of 2 W/m. There is no urgent change in the shape of the initial distribution. This result has been obtained by using a continuous mass flow through the bus bar.

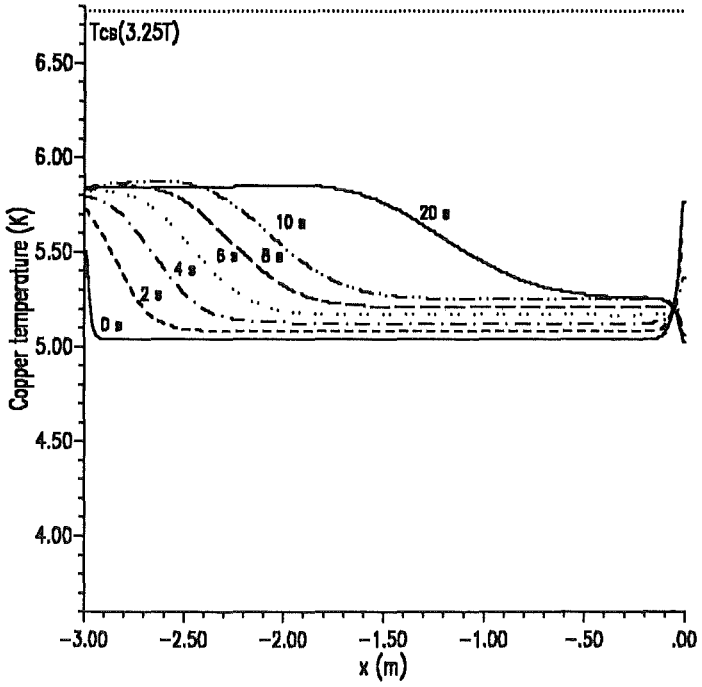

Figure 21. Temperature profiles of the conductor of the CICBUS for different times after switching off the mass flow in case of an energy dump and an external heat input of 2 W/m: A dump time constant of 3 s has been used

The conclusion is that the amount of copper in the CICBUS is too low to prevent overheating during quench.

4.7 Summary

The results of the calculations done so far for the four different bus bar designs, lead to the following conclusions

1. Steady state operation:
   all four designs only operate with contact resistances between the bus bar and the current lead of 10^{-9} Ω.
2. Loss of mass flow:
   The safety margin of the bus bar strongly depends on the amount of stabilizing copper. If an energy dump immediately starts after the loss of mass flow occurred, all bus bar designs result in temperature profile changes below the current sharing region of NbTi if the eddy current losses during the discharge mode are neglected.
3. Eddy current losses during energy dump:
   If the eddy current losses during the discharge of the model coil are taken into account, the picture changes drastically. For the SCBUS, the losses are enormously high, i.e. 31 kJ for 9 s. This leads to a quench of the bus bar within 1 s. The reason is the large cross section of stabilizing copper. A segmentation of the stabilizer in a way as it was proposed for the PSI-NET-TF conductor doesn't help much because the transversal losses (the eddy current flow in longitudinal direction) are a factor of 20 higher than the longitudinal ones, i.e. segmentation would have to be done in longitudinal direction, too. Therefore, the only way to overcome the problem is to reduce the amount of copper. A reduction from $\alpha = 80$ to 15 leads to eddy current losses of more than 800 J for 9 s resulting in temperatures being in the current sharing region of the superconductor after more than 6 s. A further reduction of α, i.e. to 2.5, leads to temperatures always below the current sharing regime. As a consequence, the low copper to non-copper ratio leads to very high temperatures during quench.

5. Proposal of a superconducting bus bar (NETBUS)

The results of the calculations for the four different bus bar designs lead to a proposal for a superconducting bus bar which is based on the design of the conductor for the NET/ITER coils. The strand material is a copper stabilized NbTi wire of 0.75 mm diameter and a copper to superconductor ratio of 1.35 (F-54 wire made by Vacuumschmelze). 924 strands are cabled together in 3 stages (33 x 4 x 7). The conduit is imbedded in a stainless steel jacket. This type of bus bar is called NETBUS.

The cross section of the bus bar can be either rectangular with an aspect ratio being that of the NET conductor or quadratic. The latter one could be advantageous because the superconducting bus has to be bent in both transverse directions. Nevertheless, because the kind of cross section is of minor importance for the calculations resented here, a decision can be made taking into account both the mechanical and technical requirements as well as the manufacturing costs.

Table 17 summarizes the geometrical data of the bus bar whereas is Table 18 the strand data are given.

Parameter of NETBUS	Unit	Value
Length	m	3.0
Outer dimensions of the cable-in-conduit-conductor (CIC)	mm x mm	27.5 x 27.5
Cross section A_{CIC} (with rounded corners)	cm^2	7.472
Cross section of copper $A_{Cu\text{-}CIC}$	cm^2	2.345
Cross section of NbTi $A_{NbTi\text{-}CIC}$	cm^2	1.737
Cross section of helium $A_{He\text{-}CIC}$	cm^2	3.390
Cooled perimeter of strands P_{cool} (2/3 of strand perimeter)	cm	147.
Outer dimensions of NETBUS (with insulation, rounded corners)	mm x mm	39.5 x 39.5
Outer dimensions of NETBUS (without insulation, rounded corners)	mm x mm	36.5 x 36.5
Cross section of stainless steel jacket A_{SS} (rounded corners)	cm^2	5.636
Nominal current	kA	50
Nominal self-field	T	0.73
Design helium pressure	bar	7.5
Design helium mass flow	g/s	2.0

Table 17. General data of the NETBUS (proposal)

Parameter of strand	Unit	Value
Diameter	mm	0.75
Number of strands		924 (33 x 4 x 7)
Wetted perimeter (2/3 of strand perimeter)	m	1.470
Helium inlet temperature	K	4.5
Non-copper operational current density (4.5 K, 4.0 T)	A/mm^2	288
Copper area	mm^2	234.5
Superconductor area	mm^2	173.7
Helium area	mm^2	339.0
Void fraction	%	44
Copper : superconductor ratio, α		1.35
RRR of copper		100
ρ(T = 5.5 K, B = 3.5 T, RRR = 100)	Ωm	$3.2 \cdot 10^{-10}$
Cable space area	mm^2	747.2
Cable corner radii	mm	3
Cable aspect ratio		1 : 1
Conductor critical current (4.5 K, 4.0 T) (5.5 K, 4.0 T) (5.5 K, 5.6 T)	 kA kA kA	 388.6 269.2 181.2

Table 18. General strand data of the NETBUS (proposal)

Figure 22 shows a cross sectional view of the NETBUS.

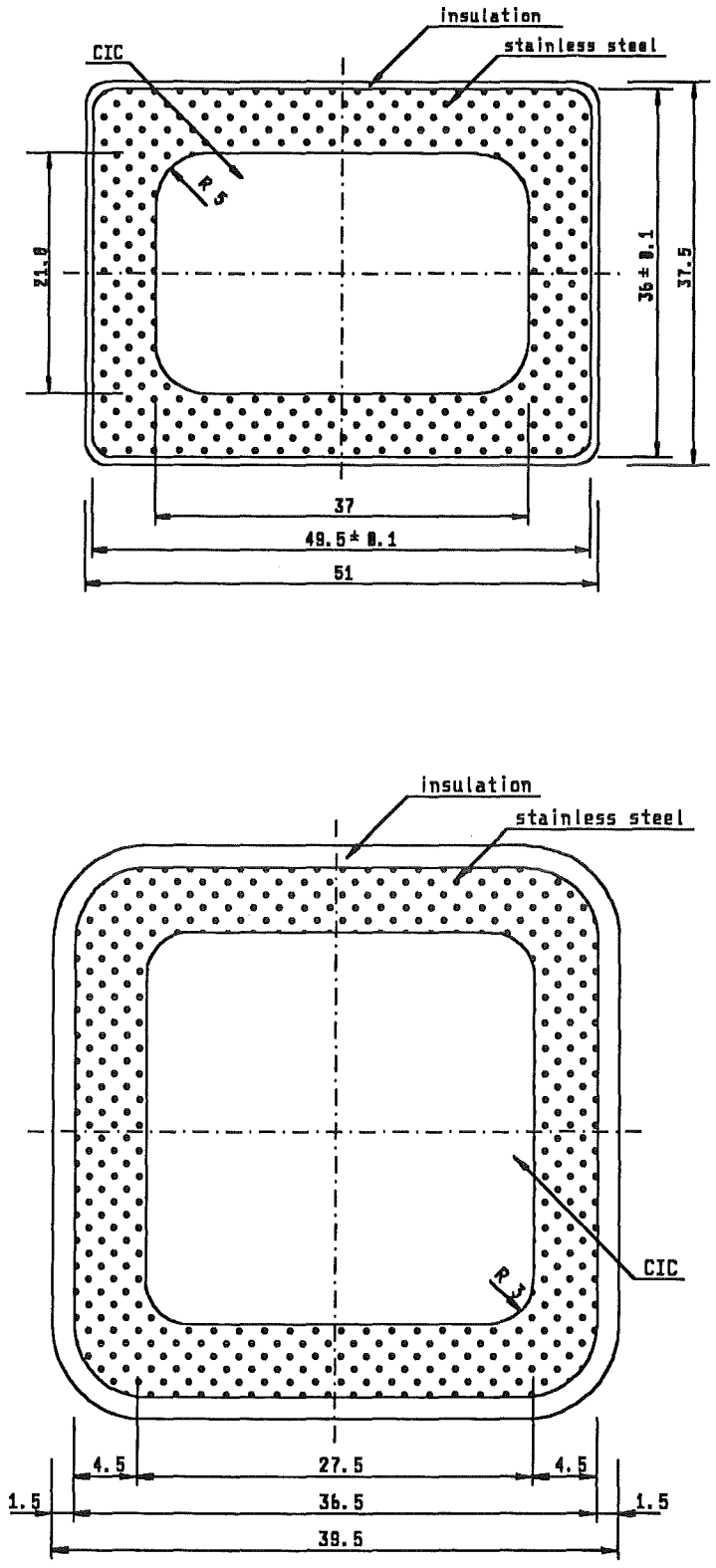

Figure 22. Transversal cross section of the superconducting bus bar NETBUS: The upper one has the rectangular cross section (NET/ITER conductor) the lower one has a quadratic cross section

5.1 Calculation results

At first, the temperature profile of the bus bar has been computed, again for contact resistivities of 10^{-9} Ω, a helium mass flow rate of 2 g/s, and a nominal current of 50 kA. Figure 23 shows the profile. For comparison, the temperature profile of the bus bars of the last sections have been plotted, too. Table 19 shows the computational results of the temperature profile calculations. For comparison, the results for the SCBUS, LCOBUS and CICBUS have been added.

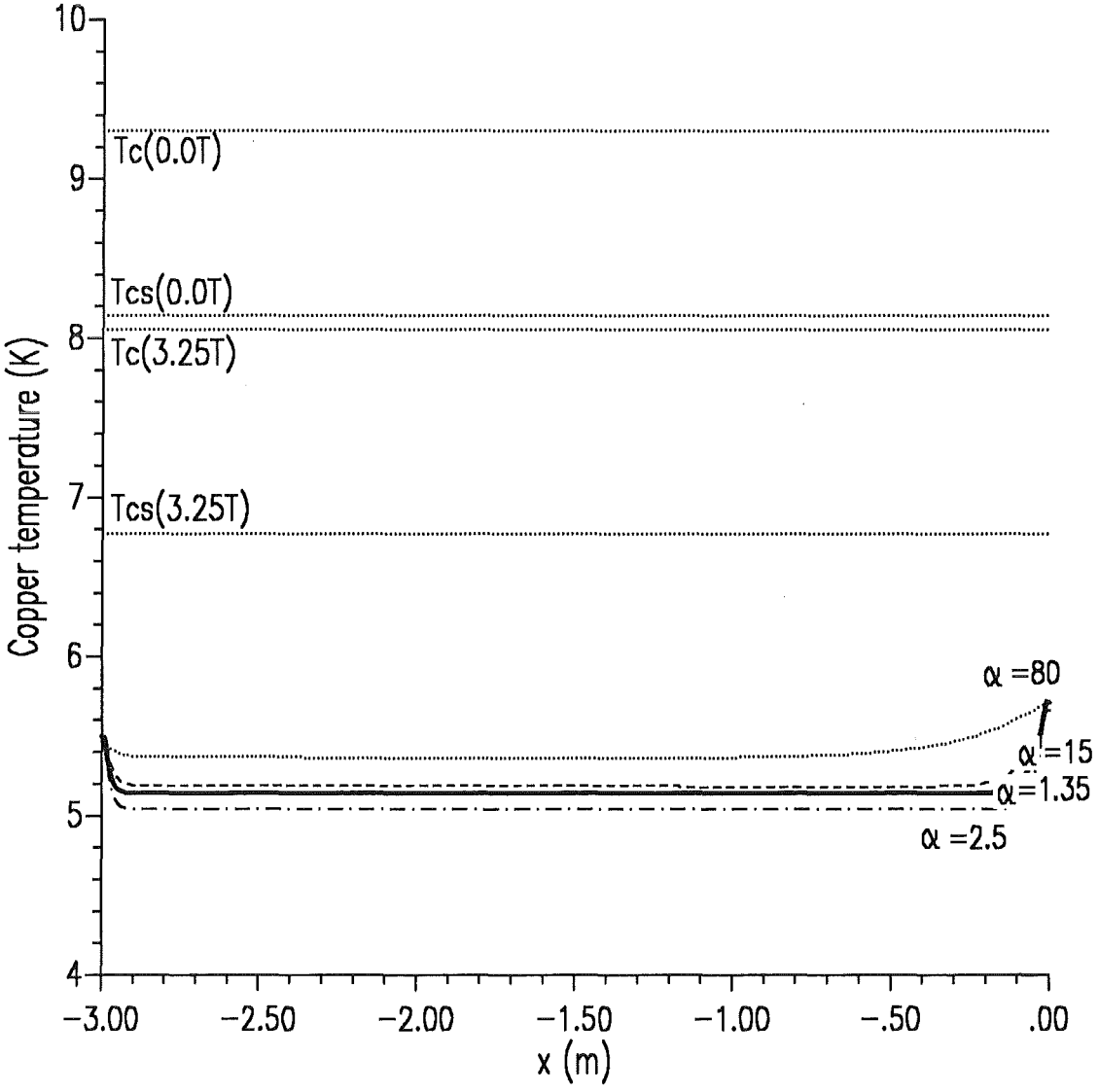

Figure 23. Temperature profile of the conductor of the NETBUS: The related profile has been ploted as a full line whereas the dotted line corresponds to the SCBUS, the dash-dotted line to the LCOBUS, and the the dashed line to the CICBUS

R_1 R_2	$\dot{m}$	ΔU	Q_{bottom}	Q_{top}	$T_{top,Cu}$	$T_{top,He}$	$T_{max,Cu}$	$\dot{m}\,\Delta H$
[Ω]	[g/s]	[mV]	[W]	[W]	[K]	[K]	[K]	[W]
superconducting bus bar ($\alpha = 80$) - SCBUS -								
10^{-9} 10^{-9}	2.0	0.20	-2.03	-0.79	5.72	5.67	5.72	10.07
superconducting bus bar ($\alpha = 1.35$) - NETBUS -								
10^{-9} 10^{-9}	2.0	0.20	0.11	-0.86	5.71	5.46	5.71	8.02

Table 19. Main results of the calculations of the temperature profile for the NETBUS: The minus sign for the heat load at both ends of the NETBUS counts for the fact that the contact areas are cooled by the superconducting bus bar by heat conduction

The behaviour of the NETBUS in case of loss of mass flow has been simulated in the same way as for the SCBUS, i.e. without energy dump and with an exponential current decay with a time constant of 3 s. Figure 24 and Figure 25 show the resultant temperature profiles along the length with time as parameter.

The result is that in case of no energy dump, the conductor temperature rises to about 200 K after 20 s whereas in case of an energy dump the temperatures stay below the current sharing temperature of NbTi.

It should be mentioned that the detection of a quench of the bus bar in case of the loss of mass flow cannot be done using a level indicator for the voltage drop (quench detector) but using a flow meter because only in this case the detection delay time of about 1 s is achievable. The rise of voltage drop needs much more time because the temperature increase is smeared along a larger conductor volume than in case of an internal quench.

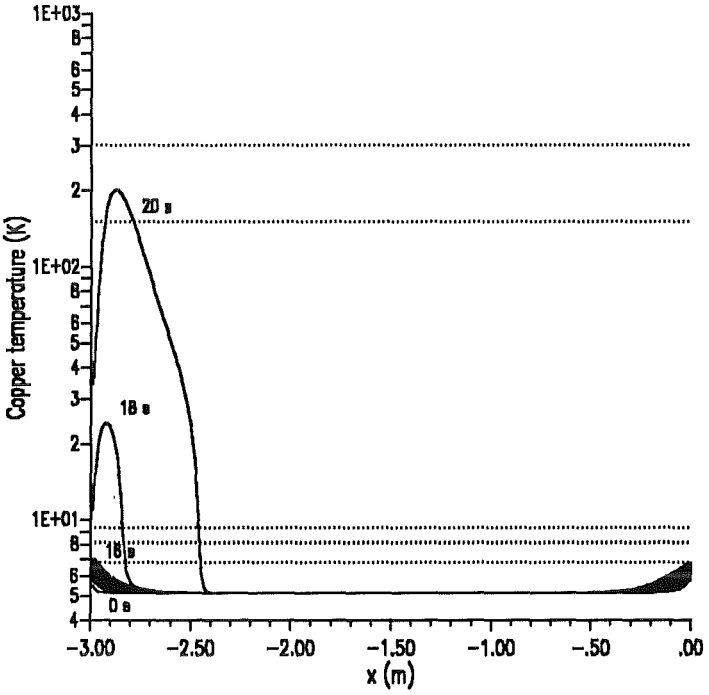

Figure 24. Temperature profiles of the conductor of the NETBUS for different times after switching off the mass flow without energy dump

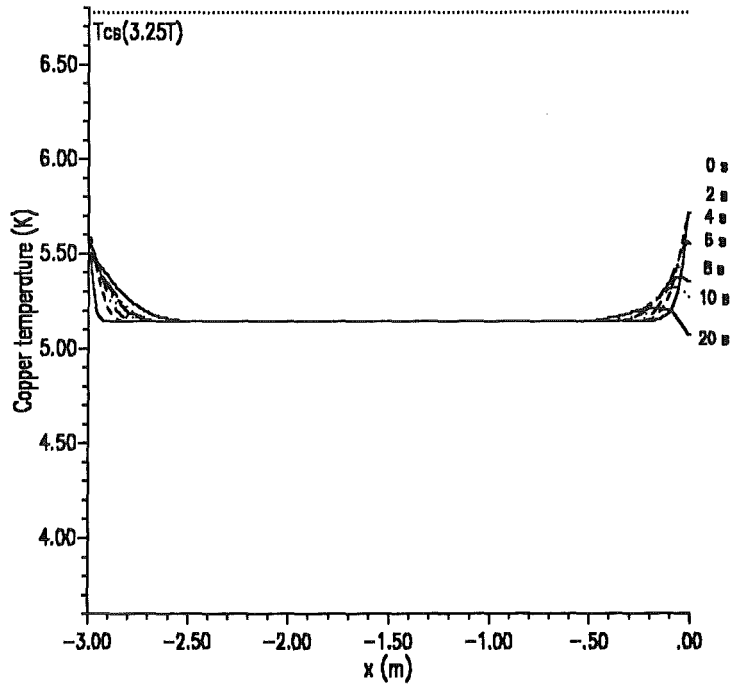

Figure 25. Temperature profiles of the conductor of the NETBUS for different times after switching off the mass flow with energy dump: A dump time constant of 3 s has been used

Now the AC-losses induced in the superconducting bus bar have been computed. Table 20 summarizes the input data for the AC-loss calculations whereas in Table 21 the resultant specific losses are presented.

Parameter	Unit	Value
Hysteresis losses		
Filament diameter d	mm	0.0670
λ		0.426
Critical current density j_c (at 3.6 T, 5.5 K) (at 2.0 T, 5.5 K)	 A/mm^2 A/mm^2	 1690. 2256.
Coupling losses		
Filament twist pitch l_f	mm	10
Twist pitch of first stage $l_{p,1}$ (estimation)	mm	350
Twist pitch of second stage $l_{p,2}$ (estimation)	mm	110
Twist pitch of third stage $l_{p,2}$ (estimation)	mm	300
Number of wires in subcable		33
Number of subcables in stage 2		4
Number of subcables in stage 3		7
Resistivity of matrix ρ_{matrix} (Cu (RRR = 100 at 3.6 T, 5.5 K)) (Cu (RRR = 100 at 2.0 T, 5.5 K))	 Ωm Ωm	 $3.2 \cdot 10^{-10}$ $2.5 \cdot 10^{-10}$
Resistivity of subcable resp. cable	Ωm	$5 \cdot 10^{-8}$
Eddy current losses		
A_{jacket}/A_{wire}		1.380696
Outer length of jacket a resp. b	mm	36.5
Inner length of jacket c resp. d	mm	27.5
Jacket resistivity ρ (stainless steel)	Ωm	$5.3 \cdot 10^{-7}$

Table 20. Geometrical input data for AC-loss calculation of the NETBUS

Parameter	Unit	Transversal	Parallel
Hysteresis losses	mJ/cm³	33.61	4.69
Coupling losses: composite 1. cable stage 2. cable stage 3. cable stage	mJ/cm³	 21.18 66.42 6.42 48.70	 6.53 20.79 2.08 15.25
Eddy current losses in the jacket	mJ/cm³	0.97	0.12
Sum	mJ/cm³ J/m	177.3 72.4	49.5 20.2
Total losses	W/m	8.04	2.24

Table 21. Average AC-losses in the NETBUS due to an exponential energy dump of the model coils

Figure 26 shows the temperature profile along the superconducting bus bar for different times after starting the energy dump which generates the AC-losses of 11 W/m. There is no urgent change in the shape of the initial distribution. This result has been obtained by using a continuous mass flow through the bus bar.

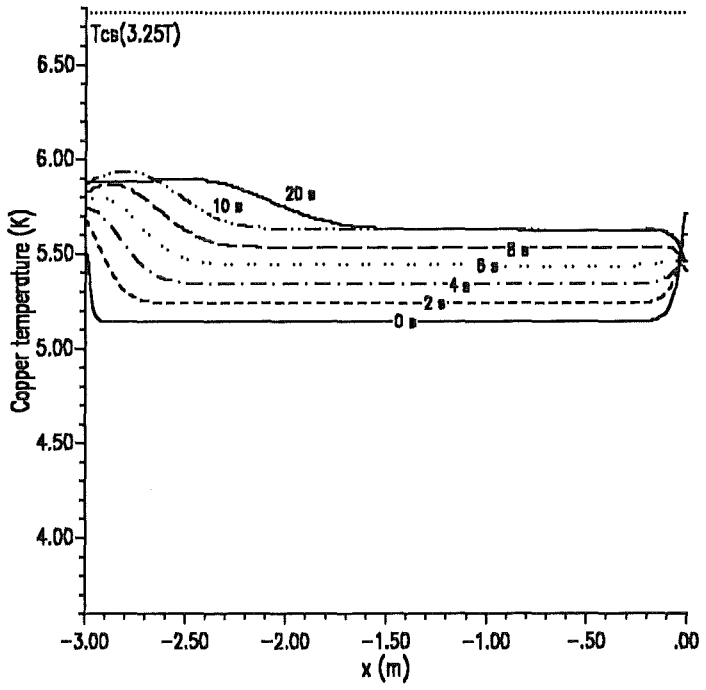

Figure 26. Temperature profiles of the conductor of the NETBUS for different times after switching off the mass flow in case of an energy dump and an external heat input of 11 W/m: A dump time constant of 3 s has been used

5.2 *Quench behaviour*

The behaviour of the superconducting bus bar in case of a quench due to an external perturbation has been simulated by means of the computer code SARUMAN-3D written by L. Bottura [13].

In the model of the bus bar, it was assumed that the stainless steel jacket has thermal contact to the conductor as well as to the helium. The cooled perimeters are assumed to be half of the inner surface of the steel jacket each.

A heat pulse of 400 W has been imposed on a length of 10 cm in the middle of the bus bar for a time of 0.5 s. After less than 100 ms, the external heat caused the superconductor to jump to the normal state. At the end of the heat pulse, i.e. 0.5 s, the temperature in the conductor has reached 30 K. After 1.5 s, the whole bus bar has quenched, resulting in a quench propagation velocity of 1 m/s.

The result is that a detectable voltage drop of 50 mV (this value was used for the EURATOM LCT-coil quench detector) has been reached after 0.7 ms. The time delay of 800 ms in total due to the dump initiation, i.e. switching off the the power supply and switching on the short circuit has been assumed in the calculations. This results in a delay time of 1.5 s after the energy perturbation had started before the energy dump of the model coil is initiated using a dump time constant of 3 s.

In Figure 27, the temperature profiles are plotted for different times after the start of the perturbation. At the time of dump initiation, the maximum temperature in the conductor is 45 K. During the following energy dump, the temperature rises to about 70 K (after 5 s) and drops then again slightly. In Figure 28 and Figure 29, the maximum temperature in the conductor resp. the voltage drop is plotted as a function of time. In these calculations, no energy input during the dump of the coil energy due to eddy currents has been imposed on the conductor for the sake of simplicity. The amount of eddy current losses is not so large that a significant change in the behaviour of the bus bar during dump would be expected.

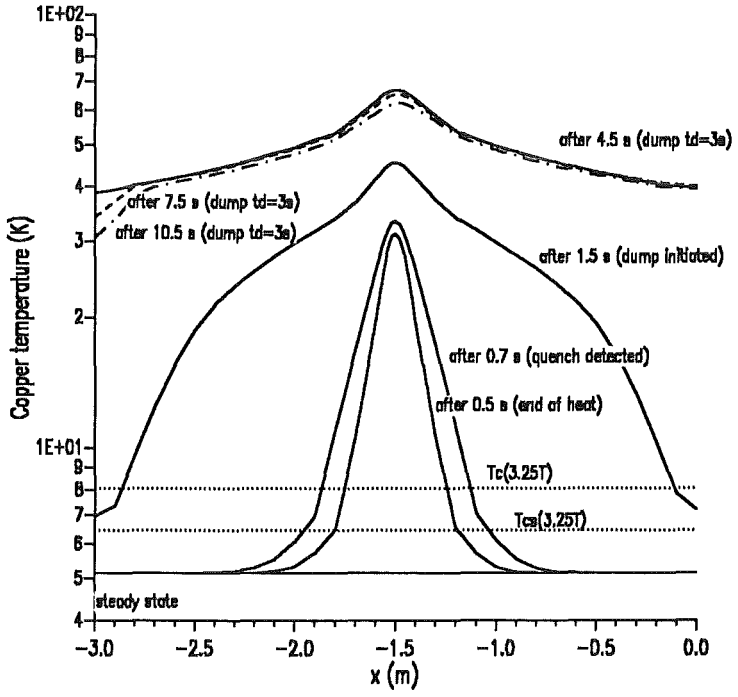

Figure 27. Temperature profiles of the conductor of the NETBUS for different times after starting the external perturbation in case of an energy dump after 1.5 s: A dump time constant of 3 s has been used

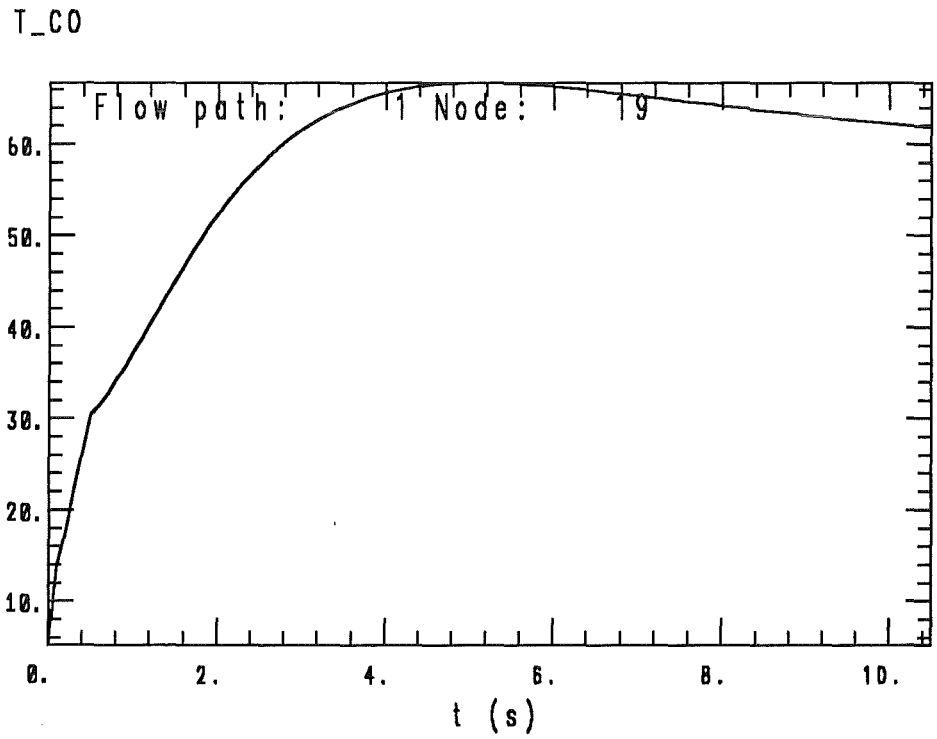

Figure 28. Maximum temperature in the conductor of the NETBUS as a function of time: A dump time constant of 3 s has been used

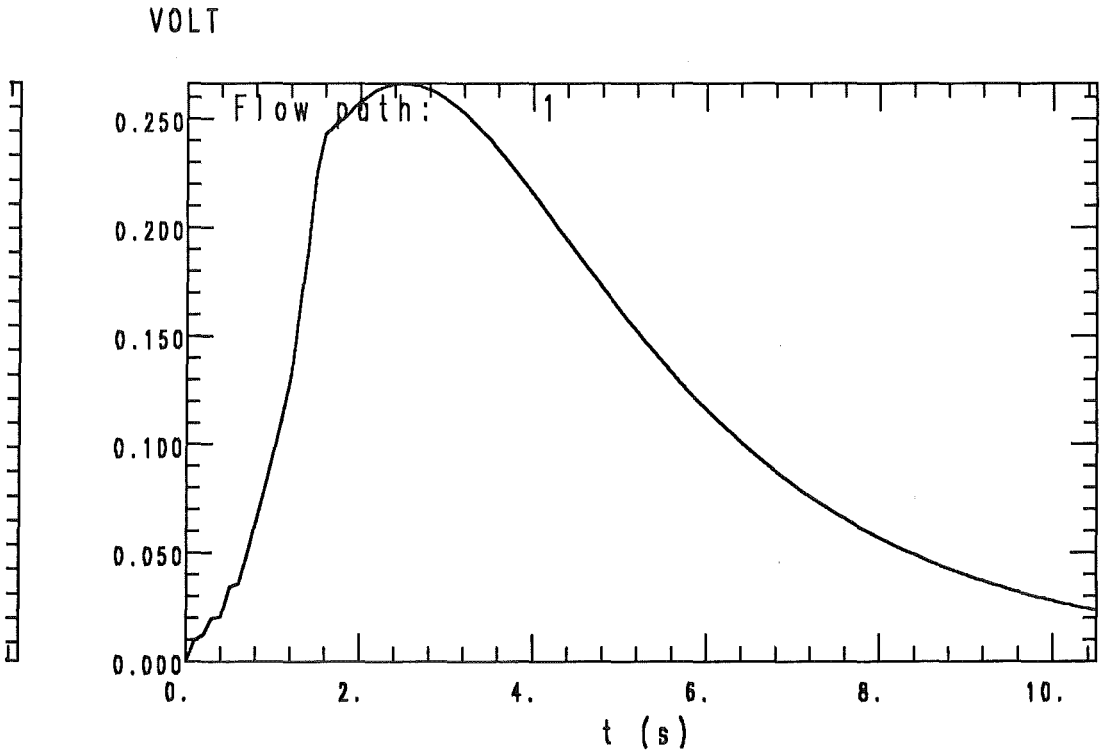

Figure 29. Voltage drop along the conductor of the NETBUS as a function of time: A dump time constant of 3 s has been used

6. Summary and conclusions

The results of the calculations done for the NETBUS will finally be compared to the ones of the other designs presented earlier.

Table 22 contains the heat load towards the model coil, the temperature of the superconducting bus bar itself, the maximum temperature of the bus (i.e. at the connector region), and the refrigerator power needed for cooling using 2 g/s of helium flow through the bus bar for all different designs. Note that all calculations base on an operating current of 50 kA, a conductor temperature at the coil end of 5.5 K, and a helium inlet temperature of 4.5 K at an inlet pressure of 7.5 bar.

	Q_{bottom} [W]	T_{bus} [K]	$T_{max,Cu}$ [K]	$\dot{m}\,\Delta H$ [W]
SCBUS ($\alpha = 80$)	-2.03	5.36	5.72	10.07
LCOBUS ($\alpha = 15$)	-0.42	5.19	5.66	8.25
CICBUS ($\alpha = 2.5$)	0.86	5.04	5.76	7.11
NETBUS ($\alpha = 1.35$)	0.11	5.14	5.71	8.02

Table 22. Main results of the calculations of the temperature profile of the different designs: The minus sign for the heat load at the end of the bus bars which is near to the coil winding counts for the fact that the contact area is cooled by the superconducting bus bar by heat conduction

Figure 30 shows the maximum temperatures at the conductor of the superconducting bus bar for all different designs in case of a loss of mass flow and no energy dump. The SCBUS and the CONIBUS result in the same curves because they have the same dimensions and physical properties except the copper-nickel coating around the copper wires. But this doesn't change the quench behaviour. The result is that in case of a loss of mass flow through the bus bar, the quench starts at the connector area which is related to the model coil. Moreover, it needs different time periods for quench, i.e. the time delay for quench detection is different depending on the amount of copper in the bus bar. In any case, the time delay between quench initiation and quench detection is much too long. **In case of loss of mass flow, a quench detection system based on the measurement of the resistive voltage may not be sufficient to protect the bus bar. This has to be detected otherwise e.g. by a flow meter.**

On the other hand in case of a quench of the superconducting bus bar due to external heat input, the quench propagation velocity is higher because the normal zone occurs in a small conductor volume and starts propagating in both directions leading to higher resistance values. Therefore, the voltage drop rises more fast with time, i.e. the time delay between quench initiation and energy dump initiation is much shorter as in case of the loss of mass flow. **In case of an internal quench, a quench detection system based on the measurement of the resistive voltage (voltage level of 50 mV) can be sufficicently used for protection.**

Figure 31 shows the AC losses in J/m for the five bus bar designs subdivided into the three contributors, i.e. hysteresis losses, coupling losses, and eddy current losses generated during a fast discharge of the model coils with a time constant of 3 s. The difference in the design 1 to 4 are only due to different eddy current losses in the stabilizer resp. jacket whereas the difference in the proposal (i.e. NETBUS) is related to all type of losses because this is a complete new design.

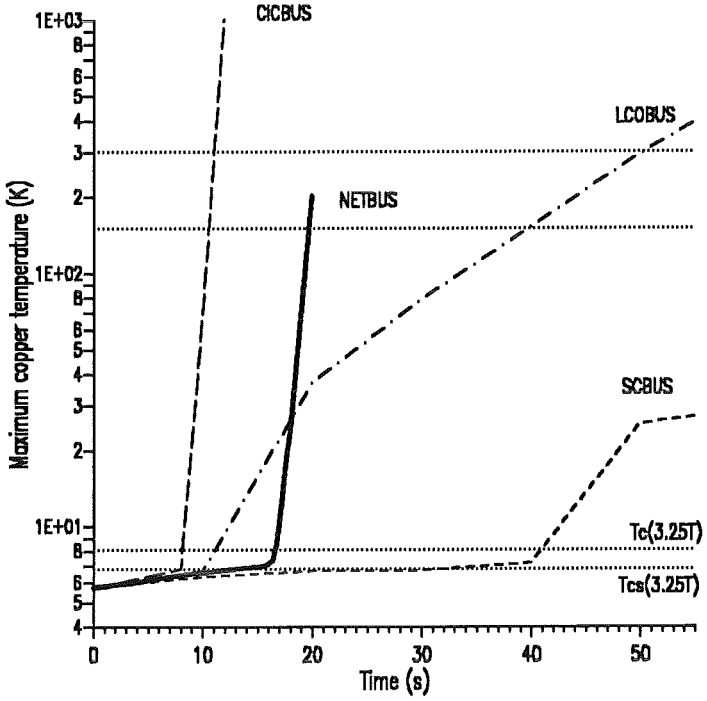

Figure 30. Maximum temperatures of the conductor of the different bus bar designs in case of a loss of mass flow and no energy dump: The SCBUS and the CONIBUS have the same curves

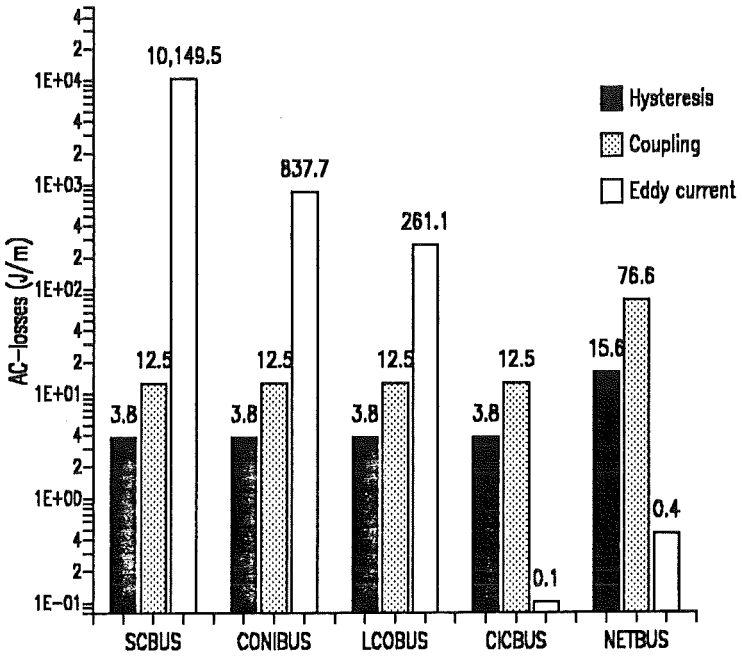

Figure 31. AC losses in J/m for all different bus bar designs: The full bars correspond to the hysteresis losses, the dotted bars to the coupling losses, and the open bars to the eddy current losses

The AC losses which are generated during the other transient field operations listed in the introduction, i.e. during plasma disruption and plasma initiation simulation as well as plasma control and divertor sweep and nuclear heating simulation are not computed because the integral field changes are lower than in case of a fast discharge. For example, a divertor sweeping simulation as proposed in [1] leads to a static heat load of about 2 mW/m which is negligible because they change the temperature of the bus bar only by 10 mK.

Concluding all the results, the superconducting bus bar for the test of the model coils (and also a possibility for NET/ITER) should be forced flow cooled NbTi cable-in-conduit-conductor of the same type as the NET/ITER coil conductor (except the type of superconductor) which has no chromium or copper-nickel coating of the strands and which is imbedded in a stainless steel jacket for mechanical stability. The cross section should be quadratic due to the bending in both transverse directions. The quench detection system of the bus bar system has to be as sensitive as for the EURATOM LCT-coil, i.e. a level of 50 mV is recommended to prevent the bus bar from overheating. This is more important if the dump time constant will be larger than the used 3 s e.g. 10 - 12 s as foreseen in NET / ITER.

An unsolved problem so far is the technical realisation of a low loss connector which requires low electrical resistances (10^{-9} Ω, i.e. large copper cross sections) and low AC losses (small copper surfaces perpendicular to the vector of high magnetic field changes).

Acknowledgement

This work has been performed within the frame of the European Fusion Technology Programme.

7. References

[1] R. Annandale, D. Besette, L. Bottura, P. Bruzzone, D. Ciazynski, H. Katheder, P. Libeyre, N. Mitchell, M. Perella, D. Robinson, E. Salpietro and B. Turck, "Concept Definition and Analysis of the NET Model Coils", NET report, N/R/0221/1/E, 22.1.1991

[2] S.J. Sackett, "EFFI, a code for calculating the electromagnetic field, force and inductance in coil systems of arbitrary geometry", LLNL, Livermore, California, UCRL-52402 (1978)

[3] G. Friesinger, R. Heller, H. Katheder, and G. Zahn, "Numerical study of a 50 kA current lead for the NET model coil test in TOSKA Upgrade", KfK 4947, (1991)

[4] M.L. Browne, H. Katheder, N. Mltchell, D. Robinson, R. Heller, L. Siewerdt, M. Süßer, A. Ulbricht, F. Wüchner, G. Zahn, "Technical specification of the TOSKA Upgrade facility for testing the ITER model coils", NET report, N/P/02239/x/A, (1991), to be published

[5] L. Bottura, "AC loss expressions and calculation procedures", NET report, N/I/3500/3/A, ITER-IL-MAG-5-0-1, 2.1.1990

[6] P. Bruzzone, "AC losses in high current superconductors for nuclear fusion magnets", Diss. ETH No. 8224, (1987)

[7] B. Turck, "Effect of the respective positions of filament burdles and stabilizing copper on coupling losses in s.c. composites", Cryogenics Vol. 22 Nr. 9, (1982), 466

[8] L.Bottura, "A collection of electrical and thermal properties for the NET conductor materials", NET report N/I/3000/1/A, 10.4.1989

[9] R. Heller, "Numerical calculation of current leads for fusion magnets", KfK 4608, (1989)

[10] ABB Schlußbericht, "Machbarkeitsstudie über einen Supraleiter für Wendelstein VII-X, ausgeführt für das Max-Planck-Institut für Plasmaphysik im Rahmen des Vertrages mit der Nummer 45 118 / SB", September 1989

[11] B. Jakob, K. Kwasnitza, C. Marinucci, G. Pasztor, and G. Vecsey, "Development and evaluation of a pre-prototype Nb_3Sn conductor for the NET-TF magnet system", PSI Technical Physics, Document-number LTP-88.10

[12] K. Kwasnitza, "Basic equations for the calculations of AC-losses in the conductor for the superconducting NET-TF-coils", SIN-Report KRYO-86-13 (1986)

[13] L. Bottura, "SARUMAN; a computer code for quench analysis of superconducting coils", SARUMAN User Manual, (1990) unpublished
L. Bottura and O.C. Zienkiewicz, "Quench analysis of large superconducting magnets. Part I: Model description", NET report N/I/3500/7/A,